What physical mechanisms cause positive subtropical low cloud feedbacks in climate models?

Mark J. Webb[1], **Adrian P. Lock**[1] **and Tomoo Ogura**[2]

[1]Met Office Hadley Centre, Fitzroy Road, Exeter, EX1 3BP, United Kingdom.
[2]National Institute for Environmental Studies, Tsukuba, Japan.

Key Points:

- Physical hypotheses for positive cumulus/stratocumulus feedbacks are tested in six climate models
- For the cases examined we rule out 4/5 mechanisms in half of the models and 3/5 in the rest
- Changes in boundary layer depth, relative humidity and humidity advection are key discriminators

Corresponding author: Mark J. Webb, `mark.webb@metoffice.gov.uk`

Abstract

We investigate positive subtropical low cloud feedback mechanisms in climate models which have performed the CMIP6/CFMIP-3 AMIP and AMIP uniform +4K experiments while saving CFMIP-3 process diagnostics on model levels. Our analysis focuses on the trade cumulus/stratocumulus transition region between California and Hawaii, where positive low cloud feedbacks are present in the JJA season. We introduce a methodology to test various positive cloud feedback mechanisms proposed in the literature as primary explanations for the low cloud responses in the models. Causal hypotheses are tested by comparing their predictions with the models' responses of clouds, cloud controlling factors, boundary layer depth and temperature/humidity tendencies to climate warming. Changes in boundary layer depth, relative humidity in the cloud layer and humidity advection at the top of the boundary layer are shown to distinguish among the hypotheses considered. For the cases examined, our approach rules out 4/5 of the mechanisms considered in half of the models and 3/5 in the remainder. We argue that unambiguously identifying the positive feedback mechanisms operating in models will in some cases require intervention experiments designed to test specific hypotheses.

Plain Language Summary

Climate models show reductions in low-level clouds with the warming climate which are poorly understood. We examine cloud changes between California and Hawaii in six climate models. We consider five possible explanations for the changes. We find that examining changes in the height of low level clouds, the humidity of the air and the rate at which dry air is mixed into the clouds from above allows us to narrow down the number of explanations compatible with each model. We propose a different, more targeted approach for narrowing down the possible explanations further in the future.

1 Introduction

Comprehensive climate models remain our most effective tools for challenging oversimplistic thinking about future changes in climate. Despite recent progress in reducing uncertainty in climate sensitivity to doubling of CO_2 (S. Sherwood et al. (2020), Masson-Delmotte et al. (2021)), cloud feedbacks still make the largest contribution to the remaining uncertainty. The WCRP assessment on climate sensitivity (S. Sherwood et al., 2020), the subsequent IPCC AR6 WGI report (Masson-Delmotte et al., 2021), and more recent studies such as Cesana and Del Genio (2021), Myers et al. (2021) and Ceppi and Nowack (2021)) have placed constraints on the magnitudes of subtropical low cloud feedbacks by relating them to observable sensitivities to cloud-controlling factors such as surface temperature and lower tropospheric stability. However, the physical mechanisms responsible for cloud feedbacks such as the reduction in low cloud cover seen in the subtropics with increasing SST are not well established. This presents a challenge when it comes to improving climate models, as there are multiple parametrizations involved which represent processes such as surface-atmosphere heat and moisture exchange, atmospheric convection, turbulence, cloud microphysics and cloud cover. Without an understanding of the physical mechanisms underlying cloud feedbacks, it is hard to know which model processes need to be targeted to improve their magnitudes for the right reasons.

The Cloud Feedback Model Intercomparison Project (CFMIP, M. J. Webb et al. (2017)) specified a suite of experiments for CMIP6 which included additional process diagnostics designed to aid the diagnosis of cloud feedback mechanisms in climate models. These included cloud, temperature and humidity variables diagnosed on the models' native vertical grids, as well as atmospheric heating and moistening rates associated with atmospheric motions, convection, radiation, turbulent mixing, and cloud processes. This work exploits these diagnostics to investigate positive subtropical low cloud feed-

Table 1. Models used in this study.

Model	Project	Reference
BCC-CSM2-MR	CFMIP-3/CMIP6	Wu, Lu, et al. (2019)
CESM2	CFMIP-3/CMIP6	Gettelman et al. (2019)
HadGEM3-GC3.1-LL	CFMIP-3/CMIP6	Kuhlbrodt et al. (2018)
IPSL-CM6A-LR	CFMIP-3/CMIP6	Boucher et al. (2020)
MIROC6	CFMIP-3/CMIP6	Tatebe et al. (2019)
MRI-ESM2.0	CFMIP-3/CMIP6	Yukimoto, Kawai, et al. (2019)

back mechanisms in the six models which provided them in the CMIP6/CFMIP-3 AMIP and AMIP +4K experiments (Table 1). We test for the presence of a number of positive cloud feedback mechanisms proposed in the literature by comparing the relative sizes of climatologically meaned changes in clouds, cloud controlling factors and tendencies with warming. The analysis focuses on the trade cumulus / stratocumulus transition region between California and Hawaii, where a positive shortwave cloud feedbacks are present in all of these models (Figure 1).

This paper is organised as follows. The results and discussion (Section 2) starts with a brief description of the choices of locations and the associated profiles of cloud fraction. Physical hypotheses for positive cloud feedback mechanisms from the literature are then considered in turn, and are ruled out in cases where their predictions are incompatible with changes in boundary layer properties, near-surface properties and surface fluxes, radiative fluxes, convective and boundary layer heating and moistening rates, moist static energy tendencies and/or changes in vertical velocity and advection. We conclude by summarising our findings and discussing the implications for future work in Section 3.

2 Results and Discussion

2.1 Choice of locations and cloud profiles.

Figure 1 shows maps of changes in the climatological JJA mean shortwave cloud radiative effect (Coakley Jr and Baldwin (1984), Arking and Ziskin (1994)) between the CMIP6/CFMIP-3 amip and amip-p4K uniform +4K SST perturbation experiments described in M. J. Webb et al. (2017). Changes in this quantity can be seen as a simple measure of the cloud feedback, allowing for certain caveats as discussed by Soden et al. (2004) and M. J. Webb and Lock (2013), and noting that the experiments here are subject to a uniform increase in SST. Locations from the GCSS/WGNE Pacific cross section (Teixeira et al., 2011) are marked with circles, and the location along the transect with the most positive feedback in each model is marked with a square. This location is [141°W,23°N] for IPSL-CM6A-LR and MIROC6, and [137°W,26°N] for the other models.

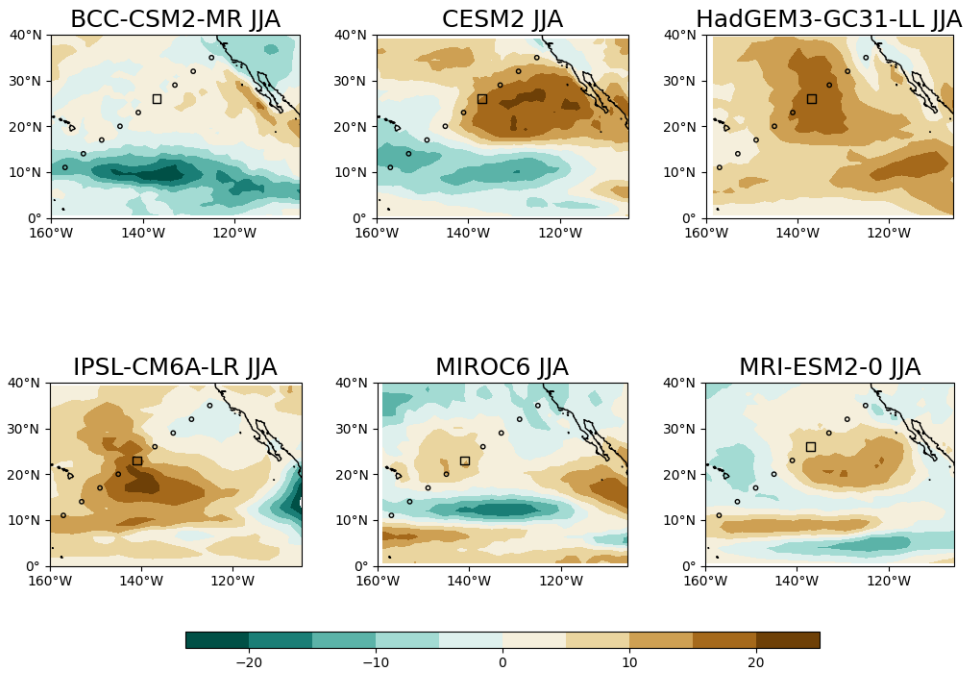

Figure 1. Climatological JJA changes in the shortwave Cloud Radiative Effect (CRE) between CFMIP-3 amip and amip-p4K experiments in the northeast tropical Pacific. Circles show locations along the GCSS/WGNE Pacific cross section (GPCI). Squares indicate locations on the GPCI with the most positive feedbacks identified for further analysis.

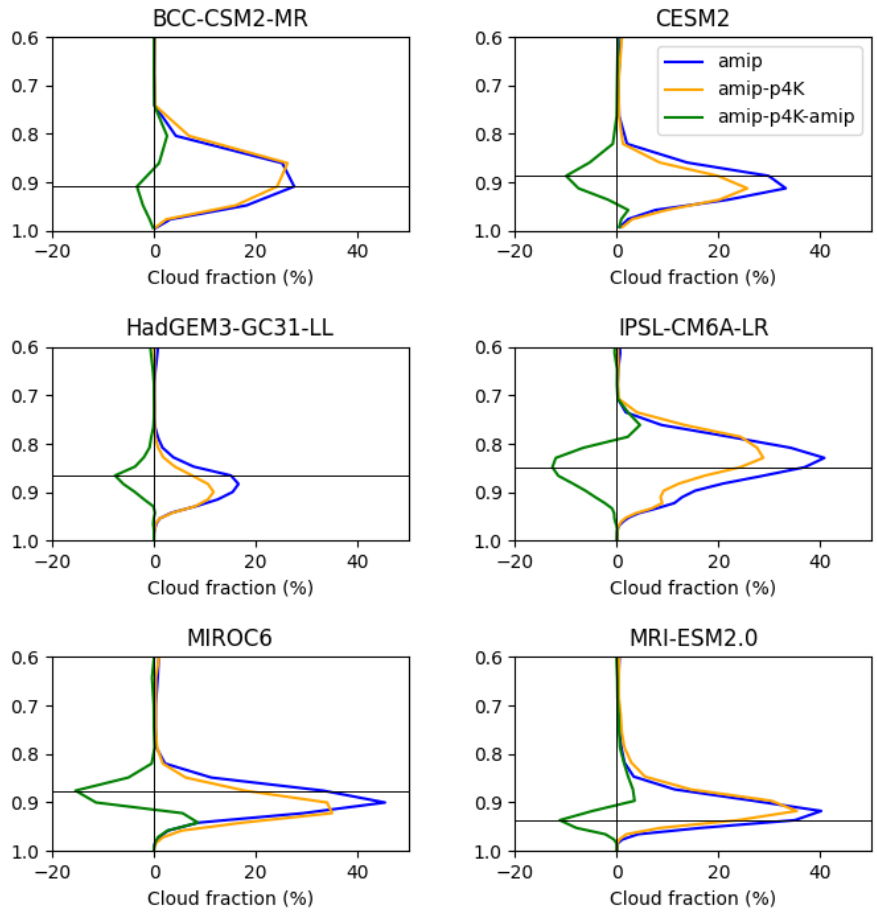

Figure 2. Cloud fraction profiles for locations indicated by squares on Figure 1. The horizontal line indicates $\sigma_{cl\downarrow}$, the level of maximum low-level cloud fraction reduction in the AMIP +4K experiment compared to the AMIP control.

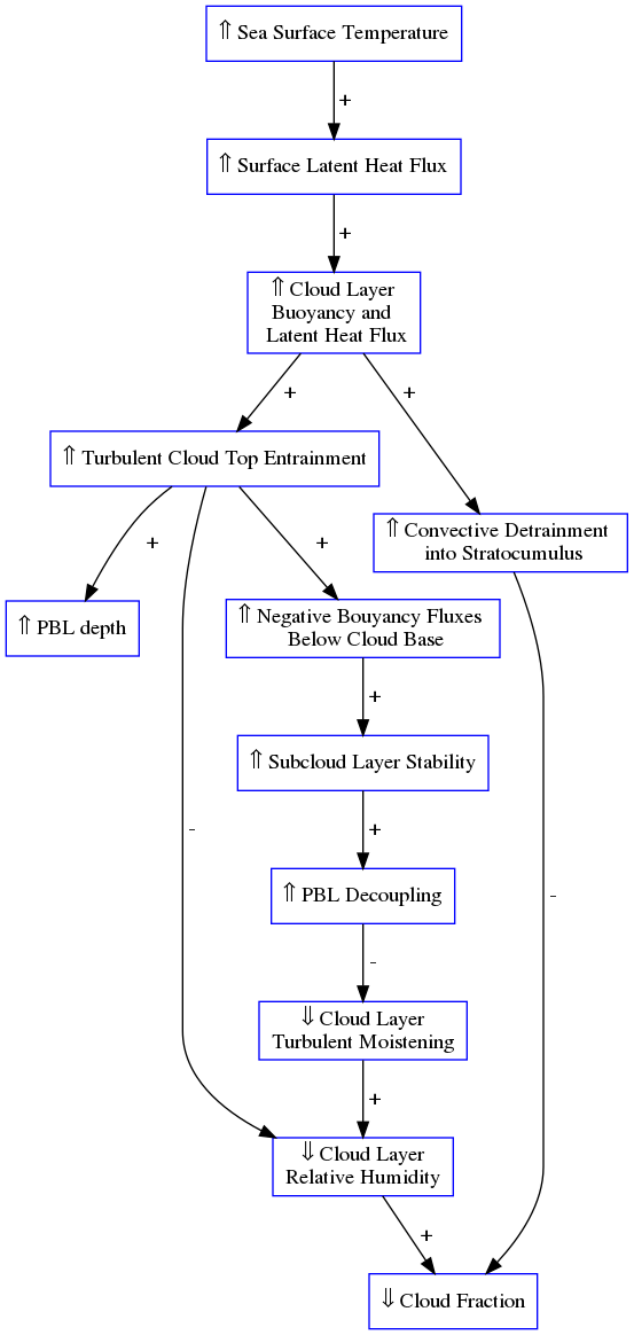

Figure 3. Summary of the surface latent heat flux decoupling mechanism. Hypothesized causal relationships where a change in one variable causes a change of the same sign in another are represented using an arrow labelled with + symbol. Those where a change of the opposite sign is caused are labelled with a - symbol.

Low cloud surface latent heat flux decoupling mechanism.	BCC-CSM2-MR	CESM2	HadGEM3-GC3.1-LL	IPSL-CM6A-LR	MIROC6	MRI-ESM2.0
Surface Temperature	0.3%	0.3%	0.3%	0.3%	0.3%	0.3%
Surface Upward Latent Heat Flux	3.8%	0.9%	2.2%	1.7%	**0.1%**	2.6%
Pressure Velocity at 700 hPa	-3.3%	-5.1%	-3.0%	-1.3%	-6.1%	-3.1%
BL depth from θ	0.2%	**-0.2%**	**0.0%**	2.9%	**-0.2%**	5.4%
BL depth from RH	0.5%	**-4.6%**	**-0.0%**	2.9%	**-4.1%**	0.5%
Potential Temperature in Cloud Layer	**0.3%**	0.5%	0.4%	0.4%	0.5%	0.4%
Relative Humidity in Cloud Layer	**0.8%**	-2.5%	-0.4%	**0.3%**	-2.2%	**0.0%**
Cloud fraction (%)	-3.0%	-8.4%	-12.6%	-8.6%	-11.6%	-8.0%
Hypothesis rejected:	**Yes**	**Yes**	**Yes**	**Yes**	**Yes**	**Yes**

Table 2. Table showing percentage changes per degree SST warming in quantities relevant to the surface latent heat flux decoupling mechanism. Values in **bold** are judged with high confidence to be inconsistent with this mechanism being the main cause of the low cloud reduction in a given model. The bottom row indicates whether or not the hypothesis is rejected for a given model.

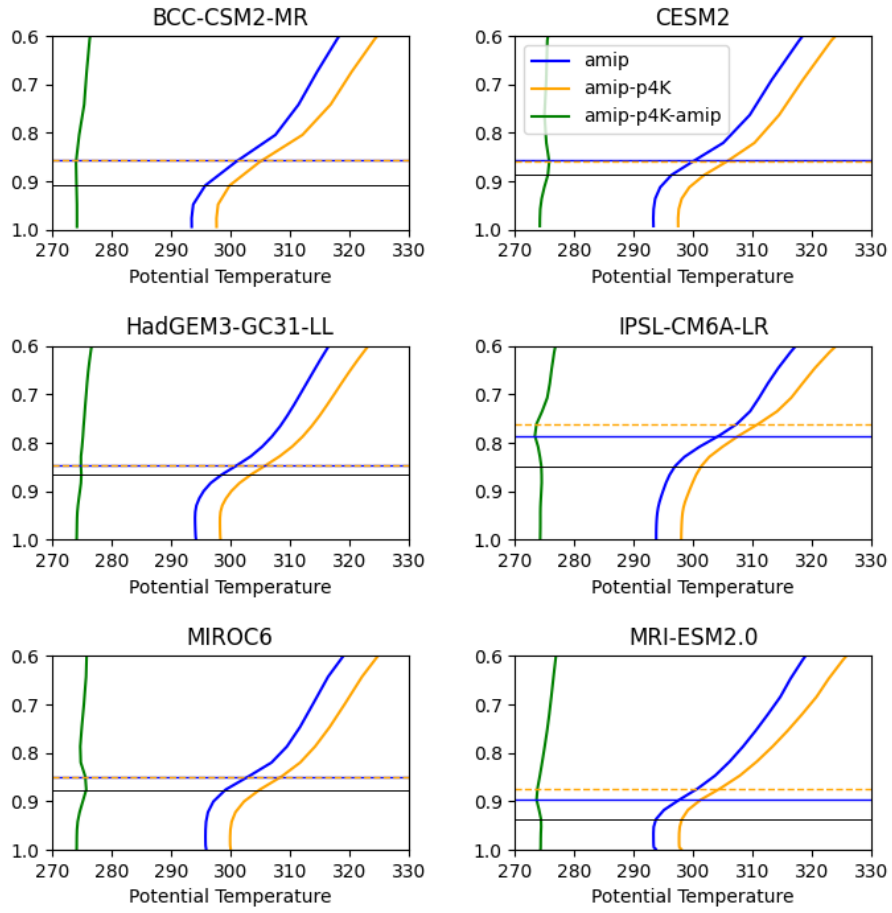

Figure 4. As Figure 2 but for potential temperature (K). The response curve has 270K added to it so it can be shown on the same scale. The horizontal blue solid and orange dashed lines indicate the levels of the boundary layer top for the control and +4K experiments respectively, estimated from the vertical potential gradients. The horizontal black line indicates the level of the largest cloud fraction reduction from Figure 2.

Figure 2 shows profiles of the low-level cloud fraction in the AMIP experiment and its changes in the AMIP+4K experiments with climate warming at the selected locations. The horizontal lines indicate the σ level at which the low-level cloud fraction reduces the most, $\sigma_{cl\downarrow}$. All models show reductions in the maximum low cloud fraction in the warmer climate. Reductions are more prominent near cloud top in CESM2, HadGEM3-GC3.1-LL and MIROC6 suggesting a reduction in the mean cloud top altitude, with increases at lower levels in CESM2 and MIROC6 which are suggestive of a reduction in cloud base height. BCC-CSM2-MR, IPSL-CM6A-LR and MRI-ESM2.0 on the other hand show decreases near cloud base and increases near cloud top suggesting increases in mean cloud base and top heights.

Various physical hypotheses have been proposed to explain low-level cloud reductions in the warmer climate, each of which make different predictions for how various cloud-

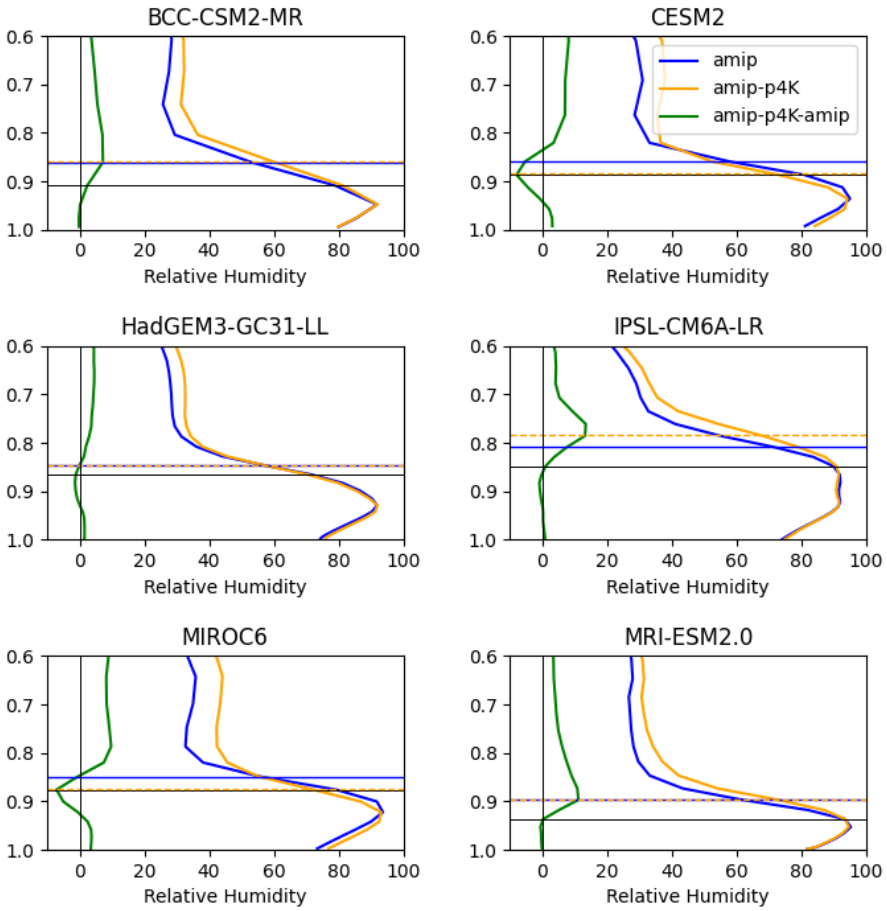

Figure 5. As Figure 2 but for relative humidity (%). The horizontal blue solid and orange dashed lines indicate the levels of the boundary layer top for the control and +4K experiments respectively, estimated from the vertical relative humidity gradients in the AMIP and +4K experiments respectively.

related quantities will change in the warmer climate. Here we consider a number of these hypotheses in turn and assess the likelihood that they explain the low-level cloud reductions shown above. This is done by testing their predictions against the model changes in cloud-layer properties, cloud controlling factors, near-surface properties, surface fluxes and temperature and humidity budget terms.

2.2 Low cloud surface latent heat flux decoupling mechanism

Wyant et al. (1997) proposed a two-stage mechanism to explain the reduction in cloud fraction observed along the stratocumulus to trade cumulus transition with increasing SST in the present climate, based on Large Eddy Simulations (LES). Here we focus on the mechanism in the first stage and will consider the mechanism in the second stage in Section 2.3.

Their initial state was a shallow, well mixed boundary layer with a positive subcloud buoyancy flux, topped by thin stratocumulus cloud. In the first stage of the transition, warming SSTs and the deepening boundary layer were accompanied by increasing surface latent heat fluxes. This was argued to increase latent heat fluxes, buoyancy fluxes and turbulence levels within the cloud, increasing the ratio of entrainment to radiative cooling. The warm entrained air was argued to lead to increasingly negative buoyancy fluxes below cloud base, creating a weak stable layer which prevented all but the strongest cumulus updraughts from penetrating the cloud base. (This argument was also supported by a mixed layer model in Bretherton and Wyant (1997).) The resulting cumulus-under-stratocumulus state was characterised by a well mixed surface layer with stratocumulus layers above which were slightly statically stable but had strong conditional stability with increasing height. The boundary layer became increasingly "decoupled", with distinct circulations in the subcloud layer and cloud layer, weakly coupled by cumulus convection. Cloud fraction remained high initially, and cumulus clouds formed which detrained into the stratocumulus.

Although cloud fraction remained high during this first transition in the Wyant et al. (1997) LES simulations, decoupling in other LES cases has been shown to result in cloud thinning and reduced liquid water paths. It is possible that GCMs with coarser vertical resolution might exhibit reduced cloud layer relative humidity in response to increased drying and heating associated with turbulent entrainment, and/or reduced turbulent moistening from below due to decoupling. This could lead to a reduction in large-scale cloud fraction in a GCM in response to decoupling. For example, Zhang et al. (2013) argued that positive cloud feedbacks were caused by enhanced turbulent cloud-top entrainment in some single column models (SCMs) run as part of the CFMIP-GASS Intercomparison of Large Eddy Simulations and Single Column Models (CGILS, Zhang et al. (2013),Blossey et al. (2013)).

Turning to climate change, Mitchell et al. (1987) and Richter and Xie (2008) argued that the bulk thermodynamic formulae employed in surface schemes in climate models are generally formulated in such a way that ensures that surface evaporation will increase at 7%/K with increasing surface temperature (in the absence of changes in relative humidity, surface wind speed, and air sea temperature differences). Rieck et al. (2012) used the same argument, and suggested that increases in surface latent heat flux in the warmer climate with a fixed relative humidity could result in a positive trade cumulus feedback, albeit following a different mechanism to the decoupling mechanism above (see below).

The stratocumulus to trade cumulus transition was argued by Wyant et al. (1997) to follow from the systematic deepening of the MBL, driven by the decrease in lower-tropospheric stability and by decreasing mean subsidence. Although weakening subsidence and its effect on boundary layer depth was considered a major factor in decoupling by Bretherton and Wyant (1997), Wyant et al. (1997) held subsidence fixed in their ex-

periments so as to highlight the effect of the SST on the stratocumulus to trade cumulus transition. They attributed the deepening of the boundary layer to the increase of the SST relative to the temperature of the free troposphere which was held fixed. This would be expected to reduce the strength of the temperature inversion at the top of the boundary layer. Based on the mixed-layer-model arguments of (Bretherton & Wyant, 1997), this would be expected to lead to an increase in entrainment of air from the free troposphere by turbulent mixing, resulting in an increase in boundary layer depth.

A causal physical hypothesis for reduced cloud fraction inspired by the first stage of the Wyant et al. (1997) mechanism plus the other considerations outlined above is presented in Figure 3. We will refer to this as the surface latent heat flux decoupling mechanism in the subsequent analysis.

We now consider the possibility that the surface latent heat flux decoupling mechanism is the main cause of the positive cloud feedbacks in each of the climate models at the selected locations. Our approach is to consider a number of changes in model variables that would have to be present if this was the case, and to rule this mechanism out as the main cause of the cloud feedback where such changes are absent. Firstly we consider the increase in the surface latent heat flux. Table 2 shows that the models all show increases significantly below the 7%/K which would be expected for an increase in SST without changes in near-surface relative humidity or wind speed. Changes in circulation and near-surface properties can result in increases in surface latent heat fluxes which are considerably smaller than 7%/K, and indeed smaller than the approximately 2-3%/K increases seen in the global mean (M. J. Webb & Lock, 2013).

The increase in surface latent heat flux in MIROC6 is just 0.1%/K. We do not consider it credible that an increase of this magnitude could be the main cause of a reduction of cloud fraction of 11.6%/K, as it is more than a factor of a hundred smaller in percentage terms. (For comparison, the LES simulations of Wyant et al. (1997) showed increases in surface evaporation of 15.7%/K (compound) which is more than a factor of two larger than the associated reductions in cloud fraction of about 6%/K seen after six days in their simulation). For this reason, we consider it extremely unlikely the surface latent heat flux decoupling hypothesis is the main cause of the low cloud fraction reduction in MIROC6, and we so we reject it as the explanation in this case with high confidence. (Note that this is a judgement based on our subjective assessment of the evidence. Other reasonable researchers may disagree with this judgement, and we reserve the right to change our judgement if new evidence or better arguments come to light.) The other models have percentage increases in surface latent heat fluxes which are at least one tenth of their percentage low cloud fraction reductions, so at this point (based on the surface latent heat flux changes alone) we choose to remain open minded about the possibility that the surface latent heat flux decoupling mechanism is the main cause of the low cloud reduction in these models.

We now turn to the next step in the causal diagram in Figure 3, the increased latent heat flux and bouyancy flux in the cloud layer. Unfortunately the CFMIP experiments do not publish diagnostics for these quantities, or for turbulent cloud top entrainment, convective detrainment into stratocumulus or buoyancy fluxes below cloud base. The mechanism does however predict an increase in boundary layer depth in response to increased turbulent entrainment. It should be borne in mind though that the the weakening in the overturning circulation commonly seen with warming in climate models is also expected to lead to an increase in boundary layer depth. All of the models show reduced subsidence in terms of weaker vertical pressure velocities at 700 hPa (Table 2). This means that any shallowing of the boundary layer must require a reduction in turbulent entrainment, which would be incompatible with the hypothesis. Similarly weakening subsidence in the absence of any change in boundary layer depth implies a reduction in entrainment.

Boundary layer depth can be estimated from the vertical profile of the potential temperature θ (Figure 4, Table 2). The σ level of the inversion capping the boundary layer is estimated using a weighted average of the σ values for the three levels with the most negative values of $d\theta/d\sigma$, using those vertical gradients as the weights. This allows the estimated boundary layer depth to sit between model levels and so reflect small changes in boundary layer depth which would be zero in many cases if the level with the most negative vertical gradient alone was used. No evidence of a deepening boundary layer is seen in CESM2, HadGEM3-GC3.1-LL3 or MIROC6 (Figure 4, Table 2). The same is the case if we estimate the boundary layer depth from profiles of relative humidity using the three levels with the largest values of $dRH/d\sigma$ (Figure 5, Table 2). Based on this evidence we consider it extremely unlikely that the surface latent heat flux decoupling mechanism is the main cause of the low cloud reductions in these models.

We also consider the possibility that more negative buoyancy fluxes below cloud base stabilise the subcloud layer, reducing turbulent moistening from below. Stabilisation of the cloud and subcloud layer would be expected to lead to a larger increase in θ in the cloud layer than at the surface. Table 2 shows this effect to be present in most of the models, but not BCC-CSM2-MR. We therefore conclude that the surface latent heat flux decoupling mechanism is extremely unlikely to be the main cause of the low cloud reduction in BCC-CSM2-MR. Finally, we look to see if the relative humidity drops in the cloud layer in the models. Table 2 and Figure 5 indicate that relative humidity does not decrease at the $\sigma_{cl\downarrow}$ level in BCC-CSM2-MR, IPSL-CM6A-LR or MRI-ESM2.0.

In summary, we conclude that the surface latent heat flux decoupling mechanism is extremely unlikely to be the main cause of the low cloud fractions reductions in any of the models at the locations examined. BCC-CSM2-MR shows no stabilisation of the boundary layer and an increase in relative humidity in the cloud layer. IPSL-CM6A-LR also shows an increase in relative humidity in the cloud layer. CESM2, HadGEM3-GC3.1-LL3 and MIROC6 show no deepening of the boundary layer, while MIROC6 shows a very small increase in surface latent heat flux. Finally, MRI-ESM2.0 shows no reduction in relative humidity in the cloud layer.

2.3 Low cloud surface latent heat flux/convective entrainment mechanism

Wyant et al. (1997) argued that during the second stage of the stratocumulus to trade cumulus transition, as SST and surface latent heat fluxes increase further, the decoupled boundary layer allows cumulus convection to become increasingly vigorous and deeper, penetrating the trade inversion and entraining more warm/dry air from above. They argued that this evaporates liquid water in convective updraughts before they detrain, reducing the convective source term for the stratocumulus, causing to to dissipate. Their LES experiments supported this argument. Cloud base precipitation was also seen to increase as the cumulus convection became more vigorous. Although their argument related to entrainment within convective updraughts, it is also possible that warm, dry air entrained from above in areas of compensating subsidence around them might evaporate stratocumulus.

Rieck et al. (2012) used the argument that surface latent heat fluxes will increase in the warming climate to motivate LES simulations of the RICO trade cumulus case with increased SSTs, initialised with specific humidities adjusted to give the same relative humidities as at the start of their control experiment. Surface evaporation increased at approximately 6% per degree surface warming, and trade cumulus occurrence reduced. This was attributed to a deepening and drying of the boundary layer, due to increased entrainment of warm, dry air from above by convection in response to increasing surface fluxes. This mechanism is very similar to second stage of the mechanism proposed by (Wyant et al., 1997), albeit starting from a cumulus boundary layer rather than a well

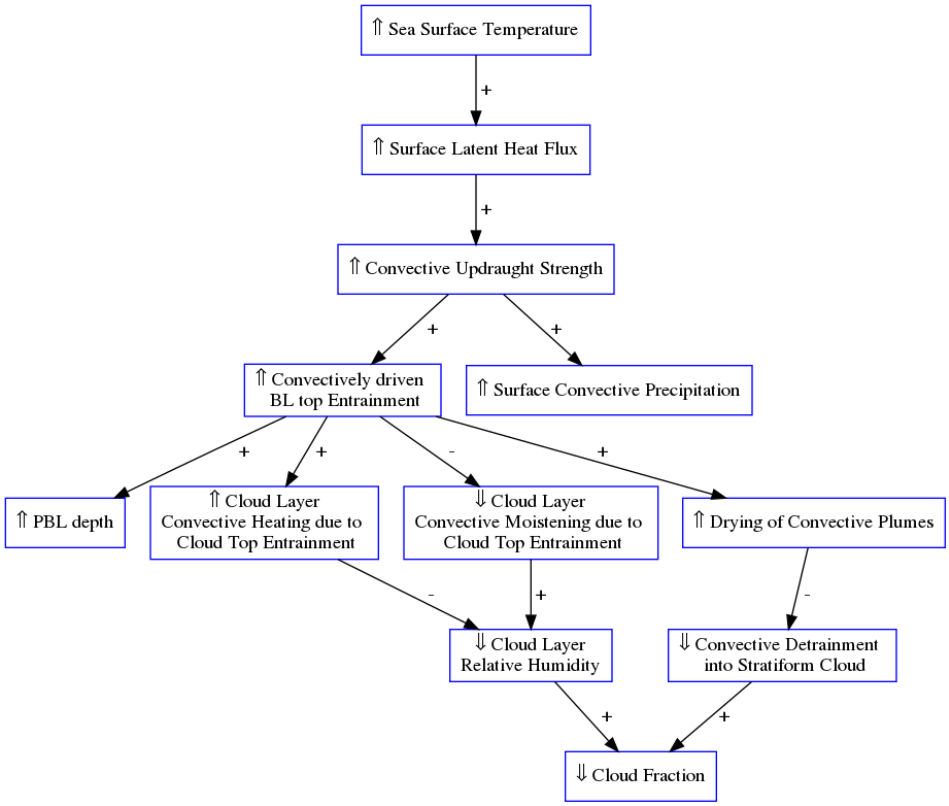

Figure 6. Summary of the surface latent heat flux/convective entrainment mechanism.

mixed stratocumulus boundary layer, and set in the context of climate warming rather than the stratocumulus to trade cumulus transition. Subsequently Zhang et al. (2013) examined positive shallow cloud feedbacks in the CGILS SCMs in cases where the shallow convection schemes were active and made the related argument that active convection could cause larger ventilation of the cloud layer in a warmer climate, leading to a decrease in cloud and a positive cloud feedback.

A causal physical hypothesis for reduced cloud fraction inspired by the second stage of the Wyant et al. (1997) mechanism, Rieck et al. (2012) and other ideas discussed above is presented in Figure 6. We will refer to this as the surface latent heat flux/convective entrainment mechanism in the subsequent analysis. If this was the main cause of the positive cloud feedback in a climate model, then we could expect to see an increase in surface evaporation, a deepening of the boundary layer and an enhanced drying or weakened moistening by parametrized convection in the cloud layer.

Table 3 summarises the model responses of quantities relevant to the surface latent heat flux/convective entrainment mechanism. We reject this mechanism as the main cause of the positive low feedback in MIROC6 because of the very small increase in surface latent heat flux (as for the surface latent heat flux decoupling mechanism). Also MIROC6 does not exhibit a deepening boundary layer or enhanced convective drying in the cloud layer. HadGEM3-GC3.1-LL shows a reduction in upward convective mass flux in the cloud layer which we consider incompatible with increasingly vigorous shallow convection. It also shows no deepening of the boundary layer, and no evidence of increased convective heating or drying of the cloud layer (Figures 7 and 8). Hence we reject the surface latent heat flux/convective entrainment mechanism as the main cause of the positive low cloud feedback seen here in HadGEM3-GC3.1-LL. Similarly we reject this hypothesis for

CESM2, on the basis of the shallowing of its boundary layer, given also that subsidence isn't increasing, as discussed in Section 2.2. The results from BCC-CSM2-MR, IPSL-CM6A-LR and MRI-ESM2.0 on the other hand are consistent with what would be expected if the surface latent heat flux/convective entrainment mechanism were the main cause of their low cloud reductions, and so this hypothesis stands as a possible explanation in these models. Although relative humidity increases in the cloud layer in some of these models, this does not rule out the possibility that stratocumulus cloud fraction reduces because of a reduced source term for large-scale cloud from the convection scheme which is not mediated by the large-scale relative humidity. Diagnostics which could rule this possibility out are not currently available from these experiments.

Low cloud surface latent heat flux/convective entrainment mechanism.	BCC-CSM2-MR	CESM2	HadGEM3-GC3.1-LL	IPSL-CM6A-LR	MIROC6	MRI-ESM2.0
Surface Temperature	0.3%	0.3%	0.3%	0.3%	0.3%	0.3%
Surface Upward Latent Heat Flux	3.8%	0.9%	2.2%	1.7%	**0.1%**	2.6%
Upward Convective Mass flux in Cloud Layer	-	-	**-6.1%**	23.6%	-	-
Convective Surface Precipitation	12.7%	4.2%	11.0%	29.9%	15.0%	18.5%
Pressure Velocity at 700 hPa	-3.3%	-5.1%	-3.0%	-1.3%	-6.1%	-3.1%
BL depth from θ	0.2%	**-0.2%**	**0.0%**	2.9%	**-0.2%**	5.4%
BL depth from RH	0.5%	**-4.6%**	**-0.0%**	2.9%	**-4.1%**	0.5%
Convective Heating Rate in Cloud Layer	1.1%	-	**-5.7%**	28.7%	0.3%	29.8%
Convective Moistening Rate in Cloud Layer	-13.0%	-4.7%	**9.9%**	-10.3%	**6.9%**	-29.9%
Relative Humidity in Cloud Layer	0.8%	-2.5%	-0.4%	0.3%	-2.2%	0.0%
Cloud fraction (%)	-3.0%	-8.4%	-12.6%	-8.6%	-11.6%	-8.0%
Hypothesis rejected:	No	**Yes**	**Yes**	No	**Yes**	No

Table 3. As Table 2 but for the surface latent heat flux/convective entrainment mechanism.

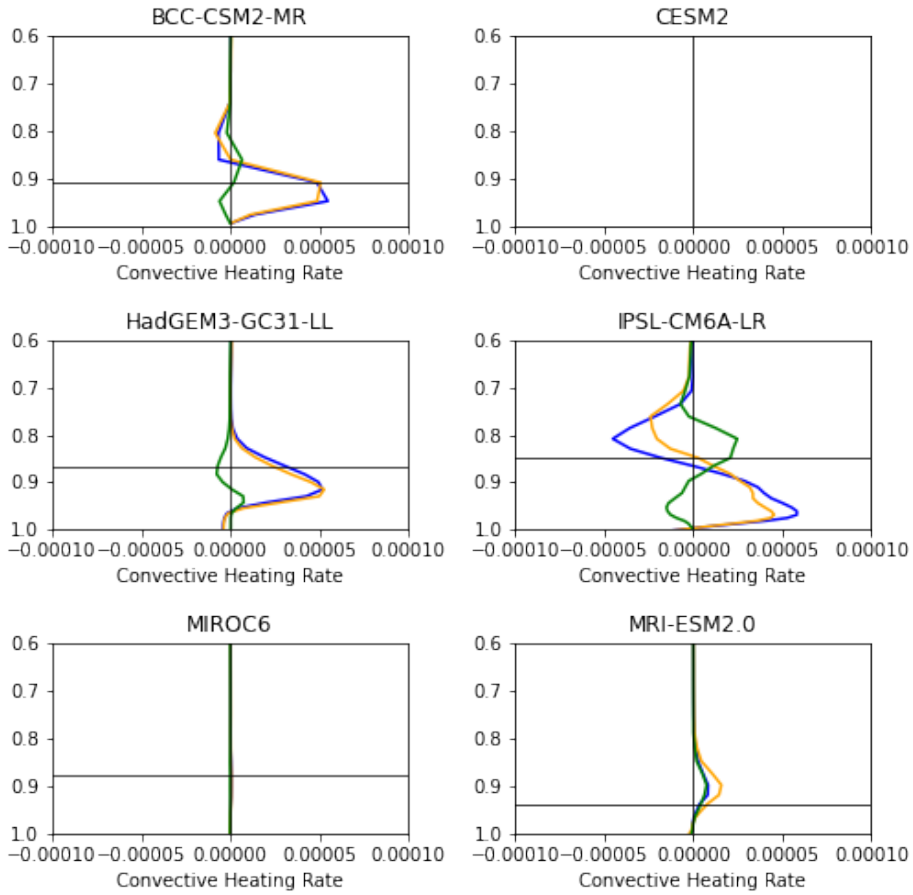

Figure 7. As Figure 2 but for convective heating rate (K/s). (No data available for CESM2).

2.4 Low cloud vertical specific humidity/MSE gradient mechanism.

Brient and Bony (2013) proposed a positive low cloud feedback mechanism based on changes in vertical gradients of specific humidity and conservation of moist static energy (MSE), a thermodynamic quantity which is a function of atmospheric temperature, humidity and potential energy. They argued that the non-linearity of the Clausius-Clapeyron relationship would cause the specific humidity (and thus MSE) to increase more near the surface than at altitude with climate warming, with changes in relative humidity playing a secondary role. This would lead to an enhanced vertical gradient of specific humidity and MSE between the PBL and the lower free troposphere, and so an enhanced source of low-MSE and dry air from the free troposphere into the PBL. This would in turn cause a reduction of low-level cloudiness in the boundary layer, weakening the longwave radiative cooling of the PBL by cloud -radiative effects which would become "less necessary" to balance the MSE budget.

Subsequently, Bretherton et al. (2013) argued that cloud thinning in LES experiments based on the CFMIP-GASS Intercomparison of Large Eddy Simulations and Single Column Models (CGILS, Blossey et al. (2013)) was caused by enhanced vertical hu-

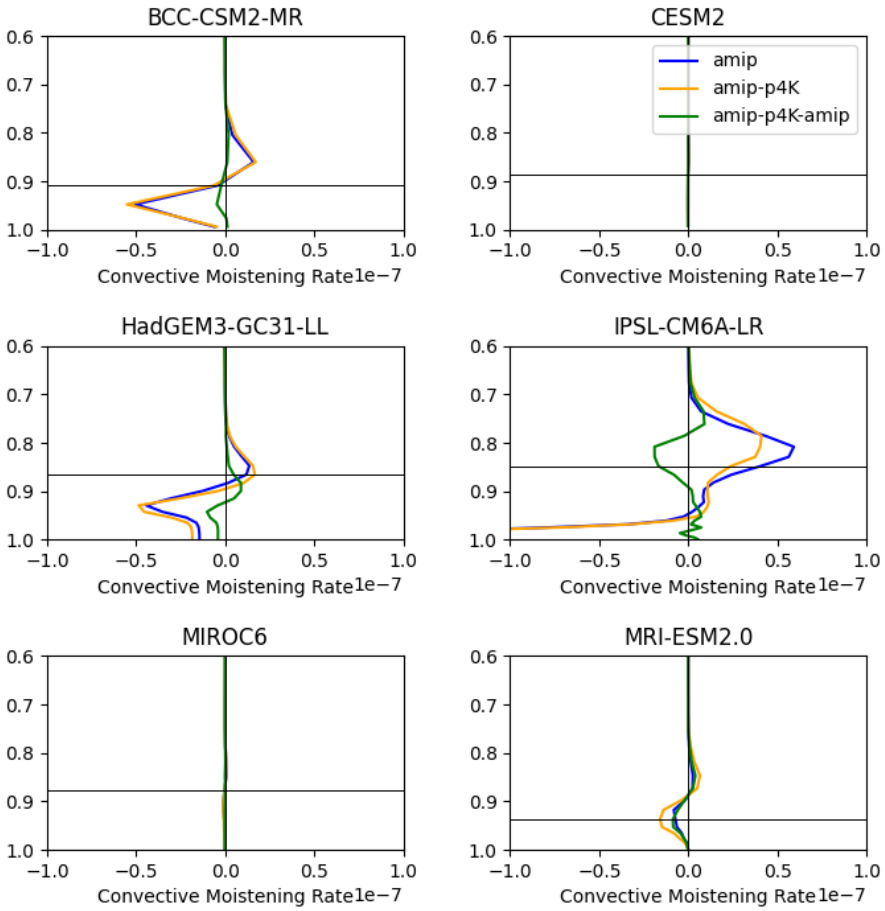

Figure 8. As Figure 2 but for convective moistening rate (kg/kg/s).

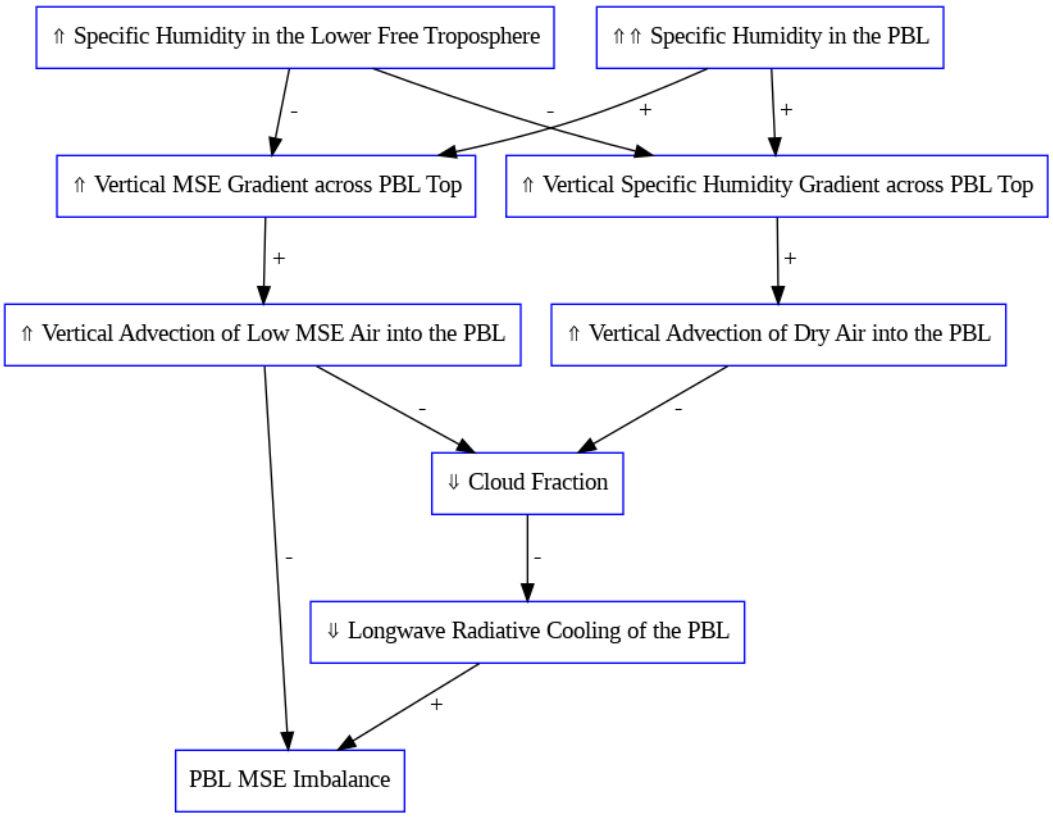

Figure 9. Summary the vertical specific humidity/MSE gradient mechanism.

midity gradients between the free troposphere and boundary layer, which allows a thinner cloud to sustain the same entrainment.

Figure 9 provides a summary of this mechanism as a causal diagram, and Table 4 summarises relevant quantities from the models. In the absence of changes in the relative humidity profile, we would expect the difference between the specific humidity in the cloud layer and at 700 hPa to increase at approximately 7%/K. Increases of around 4-5%/K are present in four of the models, but very small increases of 0.1-0.2%/K are seen in CESM2 and MIROC6, leading us the reject this hypothesis as the main explanation for the low cloud reductions in these two models (Table 4, Figure 10). Note that while Figure 10 confirms that the gross vertical gradient in specific humidity between 700 hPa and the surface increases consistently in all of the models, the changes in vertical humidity gradients at level $\sigma_{cl\downarrow}$ and near the boundary layer top are considerably more diverse.

Low cloud vertical specific humidity/MSE gradient mechanism.	BCC-CSM2-MR	CESM2	HadGEM3-GC3.1-LL	IPSL-CM6A-LR	MIROC6	MRI-ESM2.0
Cloud Layer Specific Humidity difference with 700 hPa	4.6%	**0.1%**	4.6%	5.1%	**0.2%**	5.1%
Advective Moistening Rate at PBL top	-2.8%	**3.6%**	**0.5%**	**5.2%**	**6.3%**	**3.1%**
Advective MSE Tendency at PBL top	-	**3.1%**	-4.5%	**5.1%**	**8.8%**	**6.6%**
Radiative Heating Rate in Cloud Layer	2.7%	6.1%	8.9%	11.8%	9.4%	-
Radiative MSE Tendency in Cloud Layer	2.7%	6.1%	8.9%	11.8%	9.4%	-
Cloud fraction (%)	-3.0%	-8.4%	-12.6%	-8.6%	-11.6%	-8.0%
Hypothesis rejected:	No	**Yes**	**Yes**	**Yes**	**Yes**	**Yes**

Table 4. As Table 2 but for the vertical specific humidity/MSE gradient mechanism.

The hypothesis also predicts increased drying due to vertical advection at the top of the boundary layer. Unfortunately we do not have diagnostics of the vertical humidity advection available, but we do have the total (horizontal plus vertical) specific humidity advection (Figure 11). We argue that if enhanced drying by vertical advection was to be the main cause of the cloud fraction reduction, then it would have to contribute more than changes in horizontal advection to the total. This means that in cases where there is no enhanced drying apparent in the total at the top of the boundary layer, we can rule out the hypothesis above. No such enhanced drying is present in the total at the top of the boundary layer in CESM2, HadGEM3-GC3.1-LL, IPSL-CM6A-LR or MIROC6, so we argue that the vertical specific humidity/MSE gradient mechanism cannot be the main cause of the cloud reductions in these models (Table 4, Figure 11). Note that care must be taken when interpreting changes in advective moisture tendencies when the boundary layer depth is changing. The PBL depth is increasing in IPSL-CM6A-LR and MRI-ESM2.0 which means that the advective drying increases at some levels, even though the advective drying is weaker at the BL top in the AMIP+4K experiment compared to that at the lower BL top in the AMIP experiment (Figure 11). This is a consequence of the change in BL depth, not an increase in vertical specific humidity gradient.

BCC-CSM2-MR does not provide a temperature advection diagnostic and so we don't estimate the vertical MSE advection for it. CESM2, IPSL-CM6A-LR, MIROC6 and MRI-ESM2.0 exhibit no reduction in the advective MSE tendency in the cloud layer (Table 4, Figure 12). For these reasons we rule out the low cloud vertical specific humidity/MSE gradient hypothesis as the main cause of the low cloud changes seen in all of the models except for BCC-CSM2-MR. One of the reasons why the advective MSE tendency does not reduce may be that the reductions in subsidence will act reduce the magnitude of the vertical MSE advection; this effect may compensate for or overwhelm the effects of increased vertical gradients in specific humidity.

2.5 Low cloud free-tropospheric downwelling longwave mechanism.

Based on LES experiments, Bretherton et al. (2013) argued that increases in the downwelling flux from the free-troposphere in response to increased humidity would be expected to reduce the radiative driving of turbulence in the boundary layer, resulting in cloud-top reduced entrainment, a shallowing of the boundary layer and shallowing/thinning of the cloud layer. Increases in free tropospheric specific humidity would be expected with warming if relative humidity remained constant, but would be larger if it increased. Increases in downwelling longwave fluxes are also expected in response to increasing free tropospheric temperatures, and could also be affected by changes in mid-upper level clouds. It is also possible that GCMs with coarser vertical resolution than LES might exhibit reduced cloud layer relative humidity and cloud amount instead of (or as well as) cloud thinning in response to increasing downwelling longwave fluxes. Finally, although not relevant to these experiments, we note that this mechanism is similar to those argued to explain changes in low level cloud in response to increased carbon dioxide in experiments where SSTs are held fixed (e.g. Kamae et al. (2015). This mechanism is summarised in a causal diagram in Figure 13 and relevant quantities from the models are shown in Table 5. All of models which provide the relevant diagnostics show increases in the downwelling longwave clear-sky flux and reductions in radiative cooling in the cloud layer, consistent with this hypothesis (Figures 13,14, Table 5). However BCC-CSM2-MR, HadGEM3-GC3.1-LL, IPSL-CM6A-LR and MRI-ESM2.0 show no significant shallowing of the boundary layer (Figures 4, 5, Table 5). For this reason we rule out the free-tropospheric downwelling longwave hypothesis as the main cause of the low cloud feedback in these models. The results available for CESM2 and MIROC6 are consistent with this hypothesis, and so it remains a candidate to explain the positive low cloud feedback seen in these models. (Note that at the time of writing, the sign of the downwelling longwave clear-sky flux published for IPSL-CM6A-LR appeared to be incorrect - we reversed its sign for the present analysis.)

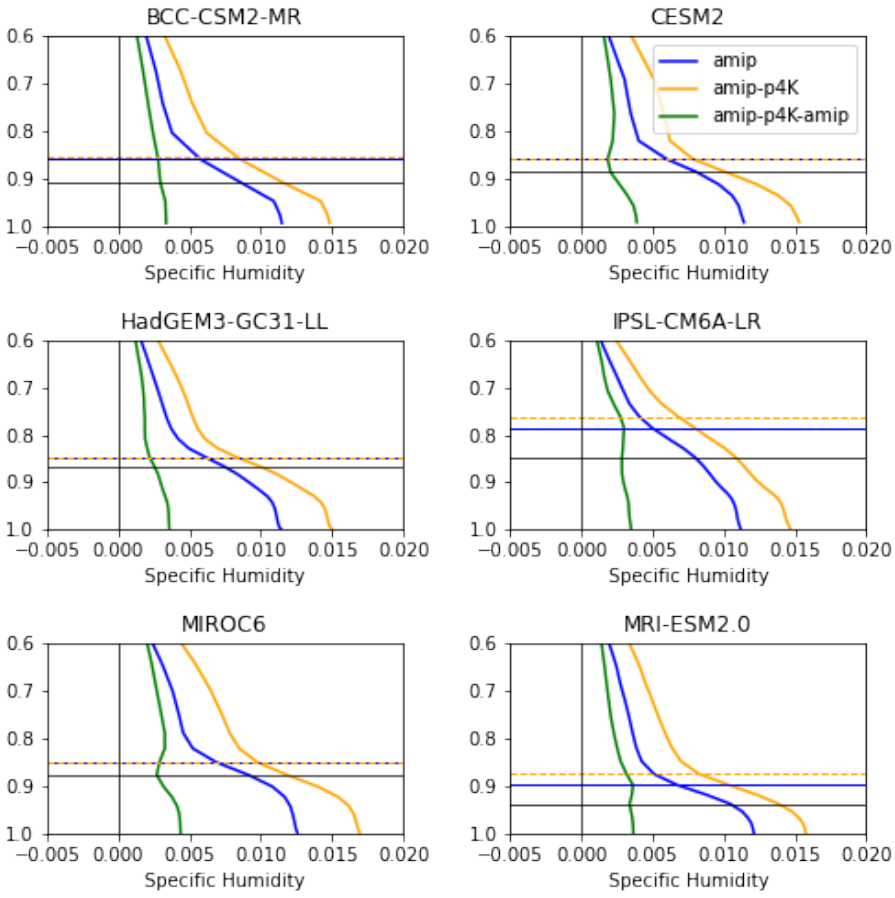

Figure 10. As Figure 4 but for specific humidity (kg/kg).

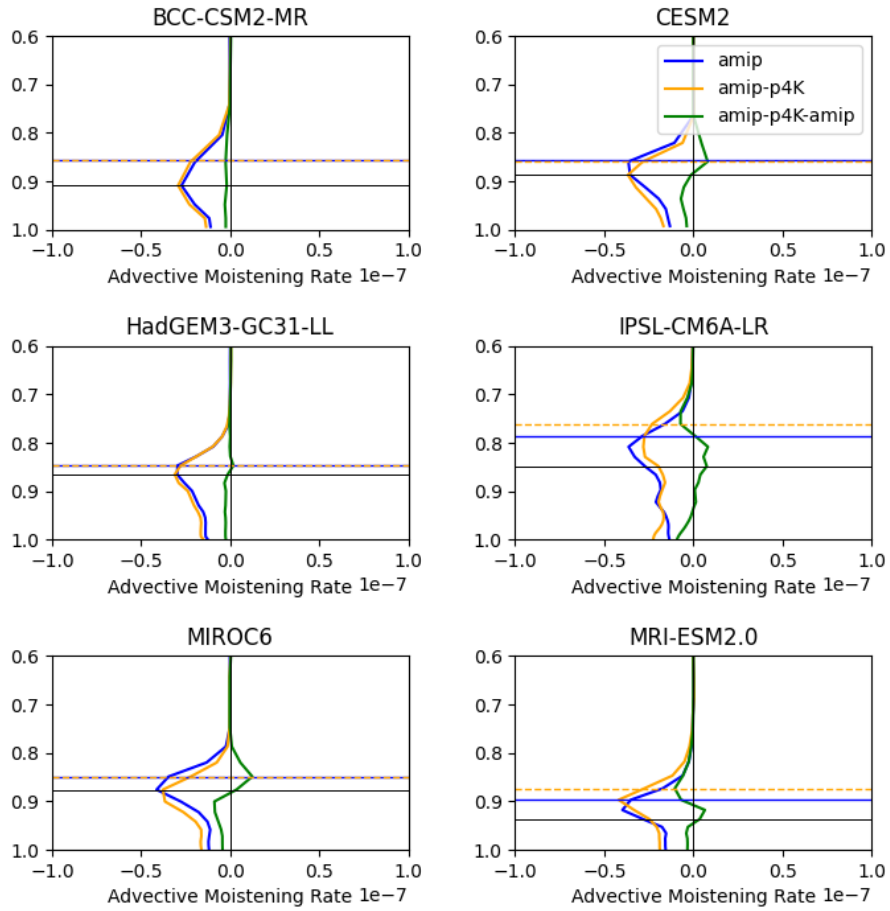

Figure 11. As Figure 2 but for advective moistening/specific humidity tendency (kg/kg/s). The horizontal blue solid and orange dashed lines indicate the levels of the boundary layer top for the control and +4K experiments respectively, estimated from the vertical potential gradients.

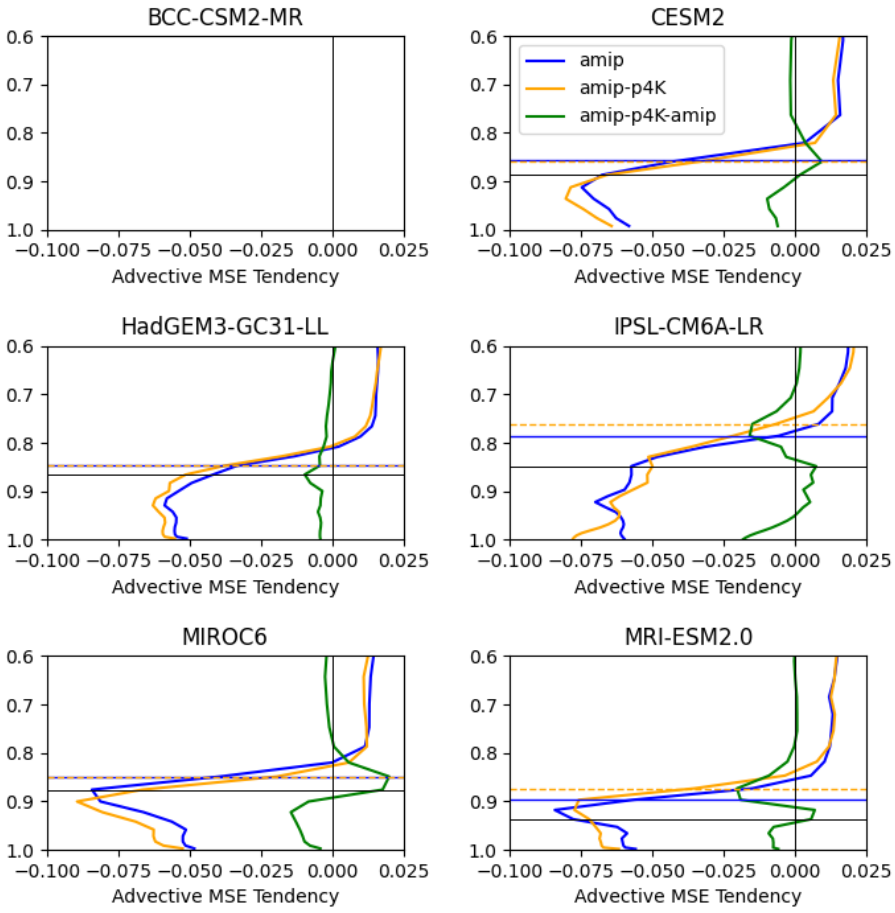

Figure 12. As Figure 11 but for advective MSE tendency (J/s). (No data available for BCC-CSM2-MR).

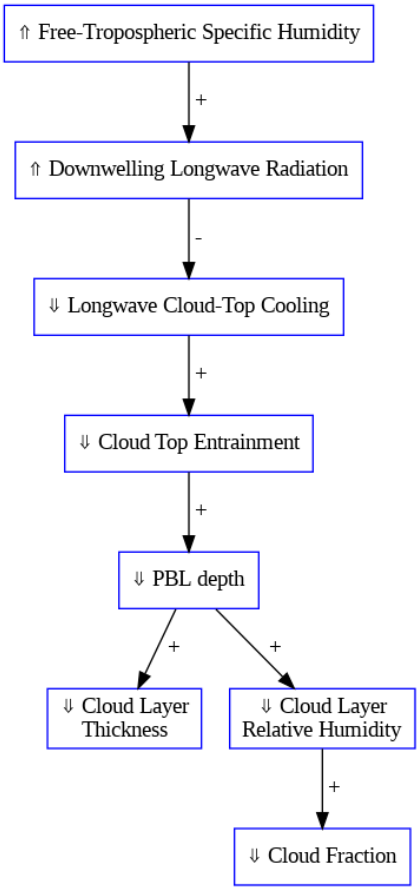

Figure 13. Summary the free-tropospheric downwelling longwave mechanism.

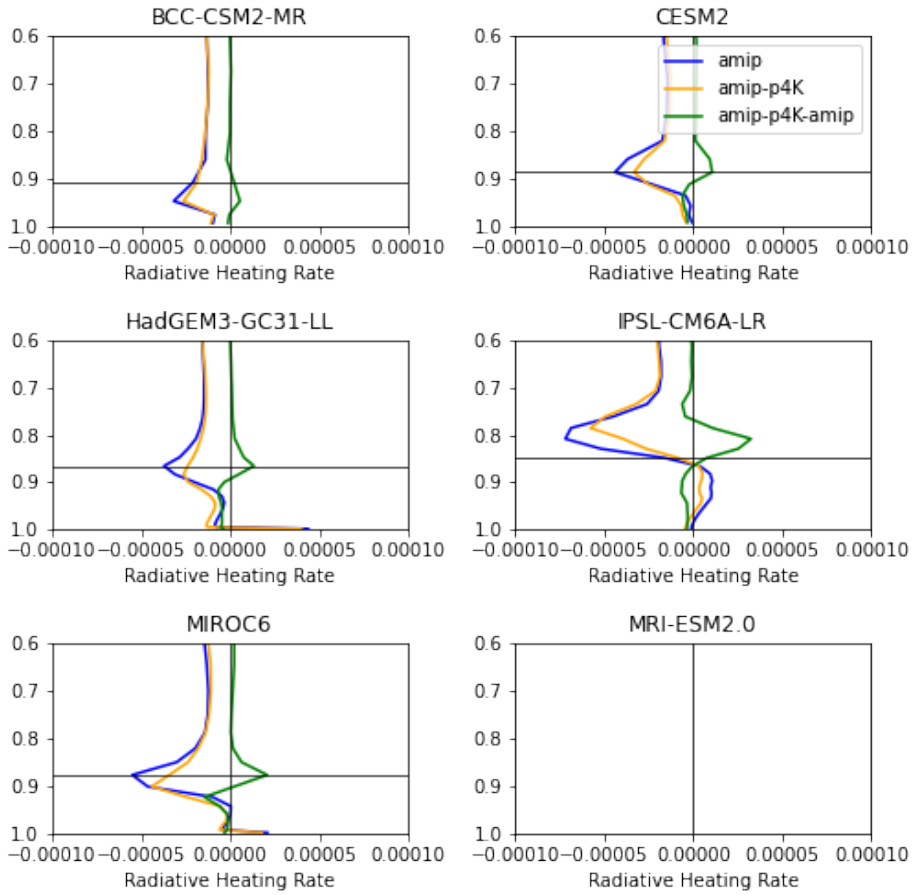

Figure 14. As Figure 2 but for radiative heating rate (K/s). (No data available for MRI-ESM2.0.)

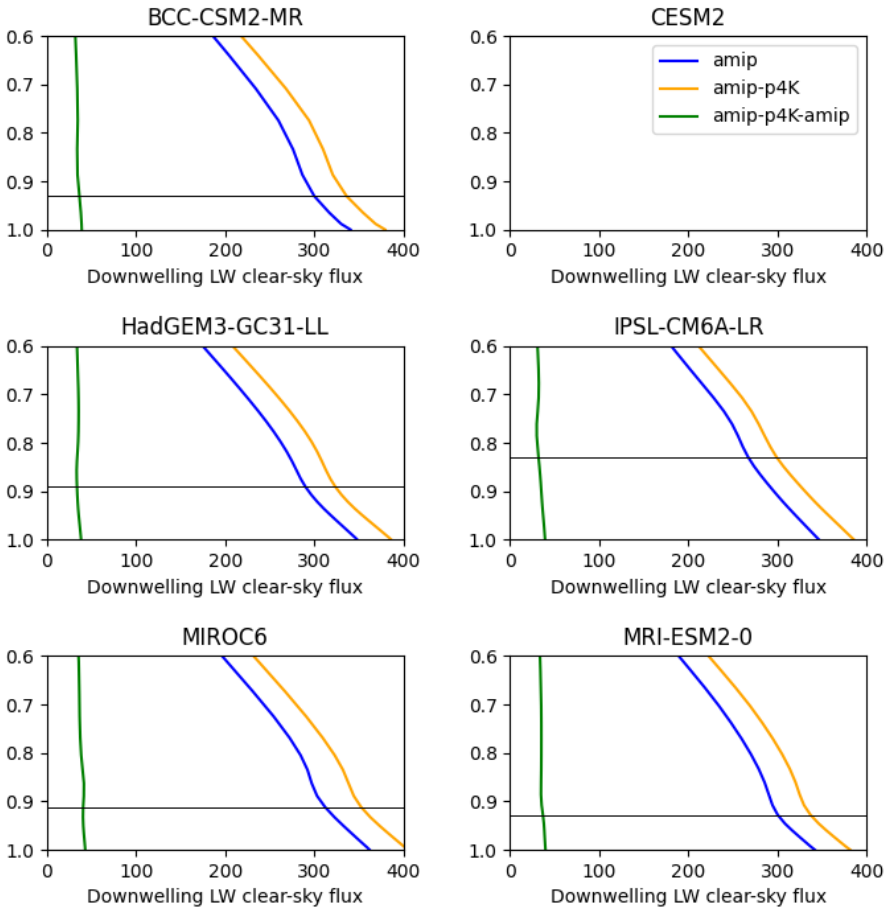

Figure 15. As Figure 2 but for clear-sky longwave downwelling radiation ($Wm^{-2}K^{-1}$). (No data available for CESM2).

Low cloud free-tropospheric downwelling longwave mechanism.	BCC-CSM2-MR	CESM2	HadGEM3-GC3.1-LL	IPSL-CM6A-LR	MIROC6	MRI-ESM2.0
Downwelling LW clear-sky flux in Cloud Layer	3.0%	-	2.9%	3.0%	3.4%	3.1%
Radiative Heating Rate in Cloud Layer	2.7%	6.1%	8.9%	11.8%	9.4%	-
BL depth from θ	**0.2%**	-0.2%	**0.0%**	**2.9%**	-0.2%	**5.4%**
BL depth from RH	**0.5%**	-4.6%	**-0.0%**	**2.9%**	-4.1%	**0.5%**
Cloud fraction (%)	-3.0%	-8.4%	-12.6%	-8.6%	-11.6%	-8.0%
Hypothesis rejected:	**Yes**	No	**Yes**	**Yes**	No	**Yes**

Table 5. As Table 2 but for the free-tropospheric downwelling longwave mechanism.

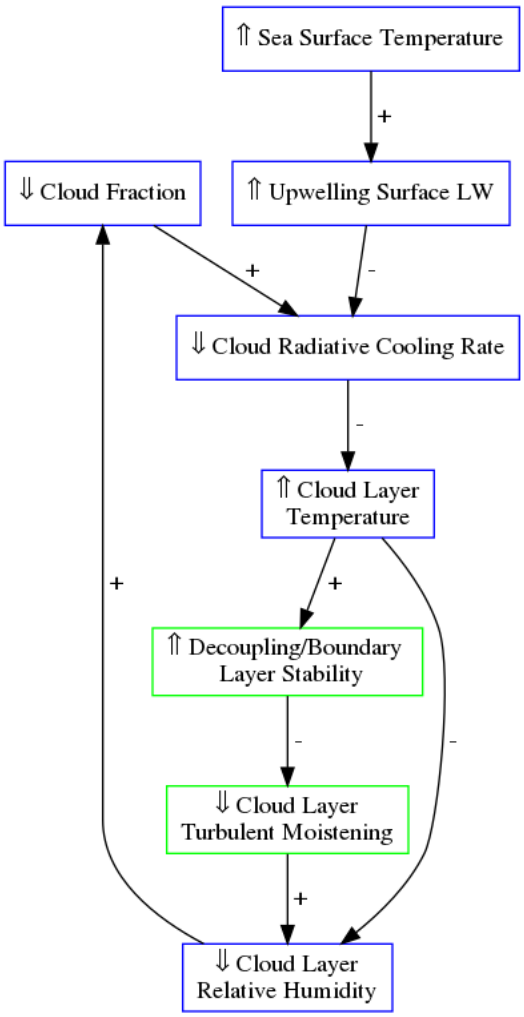

Figure 16. Summary the surface upwelling longwave mechanism. Blue boxes represent the hypothesis of Ogura et al. (submitted), while the green boxes represent a newer variant of the hypothesis incorporating boundary layer decoupling.

2.6 Low cloud surface upwelling longwave mechanism

More recently, in Ogura et al. (submitted) we proposed a new positive low-cloud feedback mechanism and demonstrated that it explained the positive subtropical low cloud feedback in the AMIP/AMIP+4K experiments performed with the MIROC5 and MIROC6 climate models. Our hypothesis was that increasing sea surface temperatures can radiatively heat the cloud layer from below, resulting in a drop in relative humidity in the cloud layer and hence a reduction in low-level cloud. This mechanism was demonstrated by performing uniform +4K SST perturbation experiments where the effects of increasing SST on radiative transfer and surface turbulent fluxes were separated. The low cloud reductions in the warmer climate were present only when the effects of increasing SSTs on the radiation were included. This mechanism is summarized by the blue boxes in the causal diagram in Figure 16.

During the present analysis we noted that the cloud layer in HadGEM3-GC3.1-LL is several model levels thick (Figure 2), and was not immediately clear to us how a radiative heating of the cloud base would lead to a reduction in relative humidity through-

out the depth of the cloud. This led us to develop a new variant of the surface upwelling longwave mechanism (green boxes, Figure 16), in which heating of the cloud base by radiation stabilises the boundary layer, resulting in a partial "decoupling" of the sub-cloud layer and the cloud layer, in turn inhibiting turbulent mixing of moisture between the sub-cloud layer and the full depth of the cloud layer. We also note that reductions in cloud fraction initially caused by the mechanism above may reduce longwave cooling of the cloud layer, warming it and reducing relative humidity further, amplifying the reduction in cloud fraction (Brient & Bony, 2012).

Relevant quantities from the models are presented in Table 6. Both variants of the surface upwelling longwave mechanism are consistent with the results shown for CESM2, HadGEM3-GC3.1-LL and MIROC6, so we are unable to rule this out as the main cause of the low cloud reductions in these models (Table 6, Figures and 14, 17 and 18). (Note that the experiments of Ogura et al. (submitted) already provide strong evidence to support this for MIROC6). However we rule this mechanism out as the main cause of the cloud reductions in BCC-CSM2-MR, IPSL-CM6A-LR and MRI-ESM2.0 as they do not show the reductions in relative humidity in the cloud layer predicted by this hypothesis (Table 6, Figure 5). Also BCC-CSM2-MR does not show any evidence to support decoupling as the cloud layer does not warm faster than the surface as expected with decoupling, and moistening of the cloud layer by the boundary layer turbulence scheme shows an increase rather than the decrease predicted (Figures 4 and 17, Table 6).

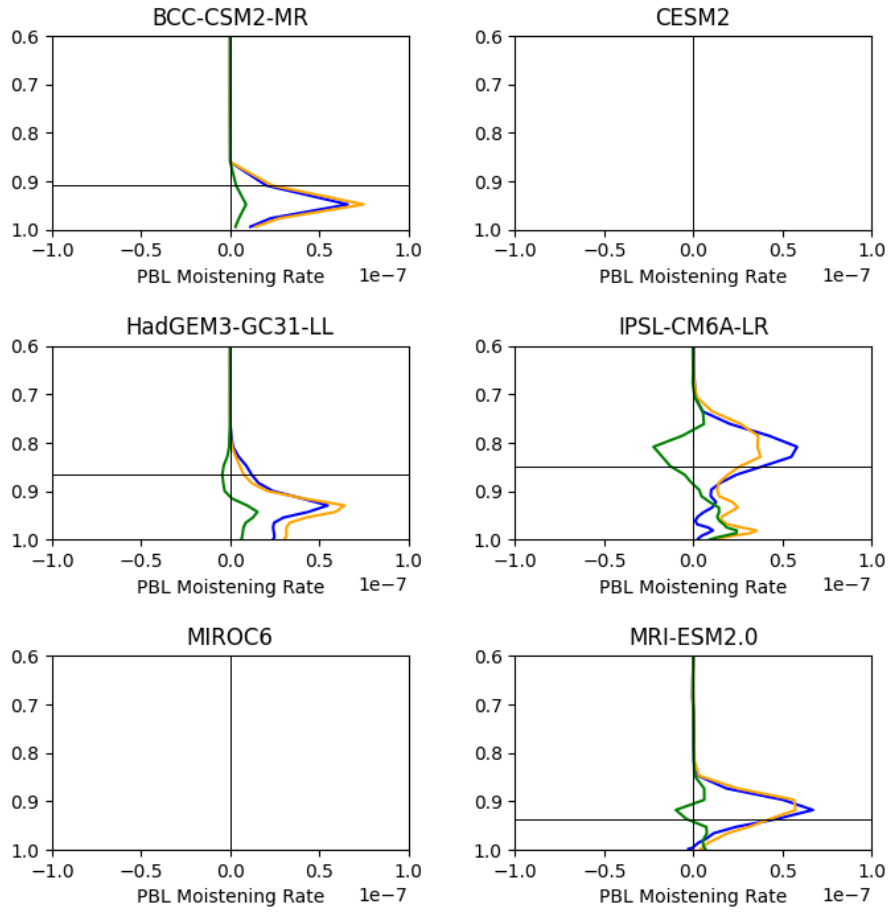

Figure 17. As Figure 2 but for boundary layer moistening rate (kg/kg/s). (No data available for CESM2 or MIROC6).

Low cloud surface upwelling longwave mechanism.	BCC-CSM2-MR	CESM2	HadGEM3-GC3.1-LL	IPSL-CM6A-LR	MIROC6	MRI-ESM2.0
Surface Temperature	0.3%	0.3%	0.3%	0.3%	0.3%	0.3%
Upwelling LW flux at surface	1.4%	1.4%	1.4%	1.4%	1.4%	1.4%
Upwelling LW clear-sky flux in Cloud Layer	1.3%	-	1.5%	1.3%	1.6%	1.4%
Upwelling LW flux in Cloud Layer	1.4%	-	1.6%	1.5%	1.7%	1.5%
Longwave Heating Rate in Cloud Layer	3.1%	6.2%	-	-	-	12.6%
Radiative Heating Rate in Cloud Layer	2.7%	6.1%	8.9%	11.8%	9.4%	-
Temperature in Cloud Layer	**0.3%**	0.5%	0.4%	0.4%	0.5%	0.4%
Potential Temperature in Cloud Layer	**0.3%**	0.5%	0.4%	0.4%	0.5%	0.4%
Boundary Layer Moistening Rate in Cloud Layer	**4.1%**	-	-9.3%	-8.2%	-	-2.0%
Relative Humidity in Cloud Layer	**0.8%**	-2.5%	-0.4%	**0.3%**	-2.2%	**0.0%**
Cloud fraction (%)	-3.0%	-8.4%	-12.6%	-8.6%	-11.6%	-8.0%
Hypothesis rejected	**Yes**	No	No	**Yes**	No	**Yes**

Table 6. As Table 2 but for the surface upwelling longwave mechanism.

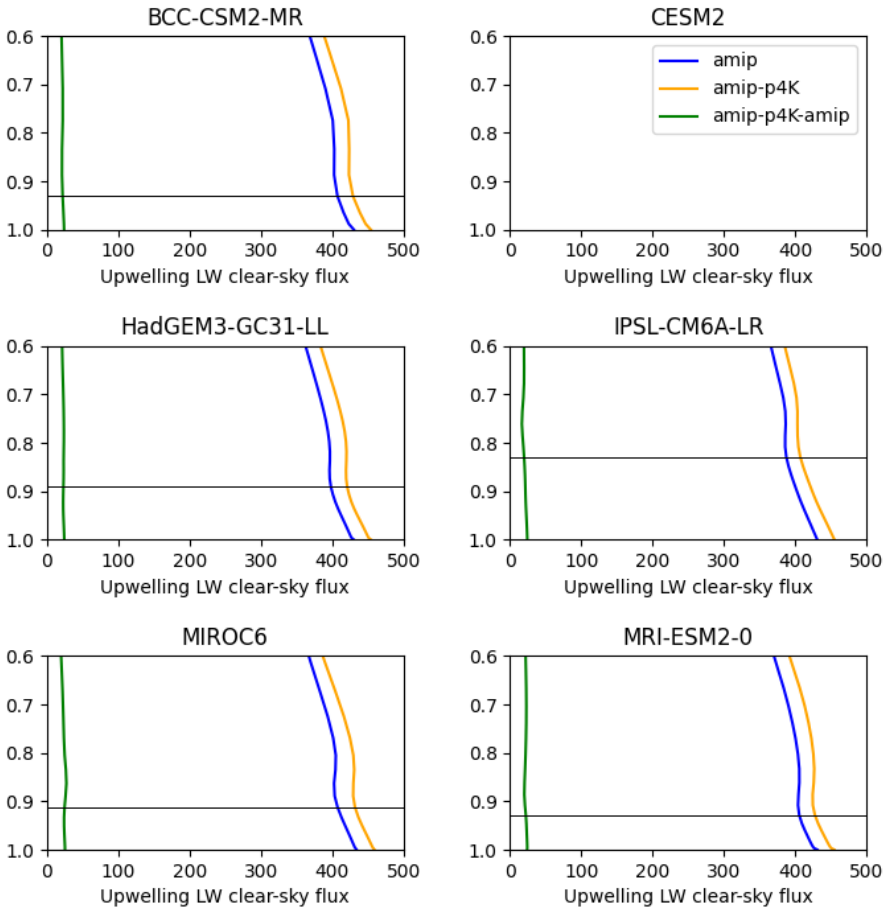

Figure 18. As Figure 2 but for clear-sky longwave upwelling radiation ($Wm^{-2}K^{-1}$). (No data available for CESM2).

3 Summary and Conclusions

Mechanism	BCC-CSM2-MR	CESM2	HadGEM3-GC3.1-LL	IPSL-CM6A-LR	MIROC6	MRI-ESM2.0
Low cloud surface latent heat flux decoupling mechanism	**No RH decrease in cloud layer; No PBL stabilisation**	**No PBL deepening**	**No PBL deepening**	**No RH decrease in cloud layer**	**No substantial increase in surface latent heat flux**	**No cloud RH decrease in cloud layer**
Low cloud surface latent heat flux/convective entrainment mechanism	Possible	**No PBL deepening**	**No PBL deepening; No convective warming and drying**	Possible	**No PBL deepening; No convective drying**	Possible
Low cloud vertical specific humidity/MSE gradient mechanism	Possible	**Increase in vertical specific humidity gradient small; No Increase in Advective Drying at BL top; No Reduction in Advective MSE tendency at BL top**	**No Increase in Advective Drying at BL top**	**No Increase in Advective Drying at BL top; No Reduction in Advective MSE tendency at BL top**	**Increase in vertical specific humidity gradient small; No Increase in Advective Drying at BL top; No Reduction in Advective MSE tendency at BL top**	**No Increase in Advective Drying at BL top ; No Reduction in Advective MSE tendency at BL top**
Low cloud free-tropospheric downwelling longwave mechanism	**No PBL shallowing**	Possible	**No PBL shallowing**	**No PBL shallowing**	Possible	**No PBL shallowing**
Low cloud surface upwelling longwave mechanism	**No RH decrease in cloud layer**	Possible	Possible	**No RH decrease in cloud layer**	Possible	**No RH decrease in cloud layer**

Table 7. Table summarising the extent to which results from the models are consistent with the various hypotheses being the main cause of their low cloud reductions. Entries in bold summarise reasons for rejecting a given hypothesis in a given model. Other entries indicate hypotheses which remain possible candidates for the main cause of the low cloud reduction in a given model.

We have investigated positive subtropical low cloud feedback mechanisms in six models which saved temperature and humidity budget terms in the CMIP6/CFMIP-3 AMIP and AMIP +4K experiments. Our analysis focuses on the trade cumulus / stratocumulus transition region between California and Hawaii at locations on the GPCI transect, where positive low cloud feedbacks are present in the JJA season. We have tested for dominant contributions from a number of positive cloud feedback mechanisms proposed in the literature by comparing the relative sizes of climatologically meaned changes in clouds, cloud controlling factors, boundary layer depth and temperature/humidity tendencies with warming.

Our findings are summarised in Table 7. We rule out all of the positive low cloud feedback mechanisms considered as the main cause of the low cloud reduction in IPSL-CM6A-LR and MRI-ESM2.0 except for the surface latent heat flux/convective entrainment mechanism of Wyant et al. (1997) and Rieck et al. (2012). For HadGEM3-GC3.1-LL we rule out all except the surface upwelling longwave mechanism of Ogura et al. (submitted). For MIROC6 and CESM2 the Ogura et al. (submitted) surface upwelling longwave and Bretherton et al. (2013) free-tropospheric downwelling longwave mechanisms are the only remaining candidates, while for BCC-CSM2-MR only the Brient and Bony (2013) vertical specific humidity/MSE gradient and Wyant et al. (1997)/Rieck et al. (2012) surface latent heat flux/convective entrainment mechanisms remain. For the cases examined, our approach has been successful in narrowing the mechanisms considered down to a single candidate for three of the six models (ruling out 4/5 of the hypotheses considered), and two mechanisms for the remaining four models (ruling out 3/5 hypotheses).

Changes in boundary layer depth, relative humidity in the cloud layer and humidity advection at the top of the boundary layer are the main factors which distinguish among the hypotheses considered. These quantities all require additional diagnostics on model levels requested in the CFMIP-3/CMIP6 experiments. As such we would consider it valuable to include these diagnostics in a wider range of experiments in future versions of CMIP, and in other model intercomparisons, for example those using storm resolving models. In this study we have not attempted to assess the credibility of the cloud feedback mechanisms in the climate models. We do however consider identifying the mechanisms operating in climate models as a useful step towards this. For example, our findings suggest that comparisons with observations that lead to improved simulations of boundary layer depth, cloud layer relative humidity and humidity advection at the top of the boundary layer could lead to more credible cloud feedbacks.

The present approach is not successful in identifying a single candidate mechanism in half of the cases examined. One possibility here is that two or more mechanisms contribute equally to the low cloud reduction. The approach we have outlined here is not able to exclude this possibility. We argue that unambiguously identifying the mechanisms responsible for positive low cloud feedbacks in such cases will require intervention experiments designed to test specific hypotheses. In future work we plan to perform climate model experiments which perturb downwelling longwave fluxes above the top of the boundary layer to test the Bretherton et al. (2013) free-tropospheric downwelling longwave mechanism, and experiments which perturb the free tropospheric specific humidity to test the (Brient & Bony, 2013) vertical specific humidity/MSE gradient mechanism. Similarly, experiments with parametrized convection deactivated (e.g. M. J. Webb et al. (2015)) may be performed to test the Wyant et al. (1997) surface latent heat flux/convective entrainment hypothesis, and further experiments separating radiative and turbulent components of SST forcing may be used to test the Ogura et al. (submitted) surface upwelling longwave mechanism in additional models.

A theoretical limitation of the present approach is that it relies on average changes. We have for instance ruled out changes in time averaged relative humidity as the main driver of reductions in cloud fraction in cases where the relative humidity increases on

average. It is of course possible that reductions in relative humidity at times when there is more cloud could cause reductions in cloud fraction, but that relative humidity could increase at other times when there is little or no cloud. In such a situation changes in the temporal distribution of relative humidity could lead to a reduction in cloud fraction even though the average relative humidity increases. This question could be investigated using high frequency model outputs saved from some CFMIP models (M. J. Webb et al., 2017). However we consider targeted intervention experiments described above to be a more fruitful approach for future work.

Clearly it would be of interest to apply this approach to other locations and seasons in these models. Also we note that some hypotheses can be excluded without reference temperature and humidity budget terms. This suggests that something may be learned about the positive cloud feedback mechanisms in other models using this approach; for instance our analysis has shown that examination of changes in boundary layer depth alone is a powerful approach for discriminating between low cloud feedback mechanisms.

Finally, we emphasize that we have not exhaustively tested all positive low cloud feedback mechanisms described in the literature. For the present study we have concentrated on those that we are most familiar with and which we are able to interpret causally. In future work we hope to consider additional hypothesized positive low cloud feedback mechanisms as explanations for stratocumulus/trade cumulus transition cloud feedbacks in climate models, for example those discussed in Brient and Bony (2012), Blossey et al. (2013), S. C. Sherwood et al. (2014), Jones et al. (2014), Vial et al. (2016), Blossey et al. (2016),Hirota et al. (2021), Koshiro et al. (2022), Schiro et al. (2022) and Vial et al. (2023).

4 Open Research

4.1 Data Availability statement

The raw CMIP6 data used in this study are archived on the ESGF (https://esgf-node.llnl.gov/search/cmip6/) and are available via the DOIs listed in the references section (see Wu, Chu, et al. (2019), Danabasoglu (2019), M. Webb (2019), Boucher et al. (2018), Ogura et al. (2019) and Yukimoto, Koshiro, et al. (2019)).

The processed CMIP6 data required to produce the figures and tables are available in a Zenodo archive available via the DOI in the reference section under M. J. Webb (2023). The code and data in this archive is accessible without restriction, and released under a BSD licence (please see the archive for further details.)

4.2 Software Availability statement

The code to download the CMIP6 data from the ESGF, process it and produce the figures and tables is available in the Zenodo archive listed in the Data Availability statement above (M. J. Webb, 2023).

This software was developed using Jupyter notebooks (https://jupyter.org/) hosted on the Google Colab platform (Bisong and Bisong (2019a), https://colab.research.google.com/). It makes use of a number of Python packages, including:

- Xarray (Hoyer and Hamman (2017), https://pypi.org/project/xarray)
- climlab (Rose (2018), https://pypi.org/project/climlab)
- pandas (McKinney et al. (2011), https://pypi.org/project/pandas)
- numpy (Oliphant et al. (2006),https://pypi.org/project/numpy)
- google-colab (Bisong and Bisong (2019a), https://pypi.org/project/google-colab/)
- matplotlib (Bisong and Bisong (2019b),https://pypi.org/project/matplotlib)

- seaborn (Bisong and Bisong (2019b),https://pypi.org/project/seaborn)
- esgf-pyclient (https://pypi.org/project/esgf-pyclient)
- IPython (https://pypi.org/project/IPython)
- cartopy (https://pypi.org/project/cartopy)
- graphviz (https://pypi.org/project/graphviz)

The manuscript was prepared using LaTeX(https://www.latex-project.org/) via Overleaf (https://www.overleaf.com).

Acknowledgments

We are grateful to Peter Blossey, Chris Bretherton, Hideaki Kawai, Jessica Vial, Zhihong Tan, Mark Ringer and Yoko Tsushima for useful discussions about this work. Mark Webb was supported by the Joint UK BEIS/Defra Met Office Hadley Centre Climate Programme (GA01101). We acknowledge the World Climate Research Programme, which, through its Working Group on Coupled Modelling, coordinated and promoted CMIP5 and CMIP6. We thank the climate modeling groups for producing and making available their model output, the Earth System Grid Federation (ESGF) for archiving the data and providing access, and the multiple funding agencies who support CMIP6 and ESGF. We are also grateful to the many authors of the Python packages which we used, listed in the software availability statement.

References

Arking, A., & Ziskin, D. (1994). Relationship between clouds and sea surface temperatures in the western tropical pacific. *Journal of climate*, *7*(6), 988–1000.

Bisong, E., & Bisong, E. (2019a). Google colaboratory. *Building machine learning and deep learning models on google cloud platform: a comprehensive guide for beginners*, 59–64.

Bisong, E., & Bisong, E. (2019b). Matplotlib and seaborn. *Building Machine Learning and Deep Learning Models on Google Cloud Platform: A Comprehensive Guide for Beginners*, 151–165.

Blossey, P. N., Bretherton, C. S., Cheng, A., Endo, S., Heus, T., Lock, A. P., & van der Dussen, J. J. (2016). Cgils phase 2 les intercomparison of response of subtropical marine low cloud regimes to co 2 quadrupling and a cmip 3 composite forcing change. *Journal of Advances in Modeling Earth Systems*, *8*(4), 1714–1726.

Blossey, P. N., Bretherton, C. S., Zhang, M., Cheng, A., Endo, S., Heus, T., ... Xu, K.-M. (2013). Marine low cloud sensitivity to an idealized climate change: The CGILS LES intercomparison. *Journal of Advances in Modeling Earth Systems*, *5*(2), 234–258.

Boucher, O., Denvil, S., Levavasseur, G., Cozic, A., Caubel, A., Foujoo ls, M.-A., ... Saint-Lu, M. (2018). [Dataset] IPSL-CM6A-LR model output prepared for CMIP6 CFMIP amip-p4K. Earth System Grid Federation. doi: https://doi.org/10.22033/ESGF/CMIP6.5126

Boucher, O., Servonnat, J., Albright, A. L., Aumont, O., Balkanski, Y., Bastrikov, V., ... others (2020). Presentation and evaluation of the ipsl-cm6a-lr climate model. *Journal of Advances in Modeling Earth Systems*, e2019MS002010.

Bretherton, C. S., Blossey, P. N., & Jones, C. R. (2013). Mechanisms of marine low cloud sensitivity to idealized climate perturbations: A single-LES exploration extending the CGILS cases. *Journal of Advances in Modeling Earth Systems*, *5*(2), 316–337.

Bretherton, C. S., & Wyant, M. C. (1997). Moisture transport, lower-tropospheric stability, and decoupling of cloud-topped boundary layers. *Journal of the at-*

mospheric sciences, *54*(1), 148–167.

Brient, F., & Bony, S. (2012). How may low-cloud radiative properties simulated in the current climate influence low-cloud feedbacks under global warming? *Geophysical Research Letters*, *39*(20).

Brient, F., & Bony, S. (2013). Interpretation of the positive low-cloud feedback predicted by a climate model under global warming. *Climate Dynamics*, *40*(9-10), 2415–2431.

Ceppi, P., & Nowack, P. (2021). Observational evidence that cloud feedback amplifies global warming. *Proceedings of the National Academy of Sciences*, *118*(30), e2026290118.

Cesana, G. V., & Del Genio, A. D. (2021). Observational constraint on cloud feedbacks suggests moderate climate sensitivity. *Nature Climate Change*, *11*(3), 213–218.

Coakley Jr, J., & Baldwin, D. (1984). Towards the objective analysis of clouds from satellite imagery data. *Journal of Climate and Applied Meteorology*, *23*(7), 1065–1099.

Danabasoglu, G. (2019). [Dataset] NCAR CESM2 model output prepared for CMIP6 CFMIP amip-p4K. Earth System Grid Federation. doi: https://doi.org/10.22033/ESGF/CMIP6.7537

Gettelman, A., Hannay, C., Bacmeister, J., Neale, R., Pendergrass, A., Danabasoglu, G., ... others (2019). High climate sensitivity in the community earth system model version 2 (cesm2). *Geophysical Research Letters*.

Hirota, N., Ogura, T., Shiogama, H., Caldwell, P., Watanabe, M., Kamae, Y., & Suzuki, K. (2021). Underestimated marine stratocumulus cloud feedback associated with overly active deep convection in models. *Environmental Research Letters*, *16*(7), 074015.

Hoyer, S., & Hamman, J. (2017). xarray: ND labeled arrays and datasets in Python. *Journal of Open Research Software*, *5*(1).

Jones, C., Bretherton, C., & Blossey, P. (2014). Fast stratocumulus time scale in mixed layer model and large eddy simulation. *Journal of Advances in Modeling Earth Systems*, *6*(1), 206–222.

Kamae, Y., Watanabe, M., Ogura, T., Yoshimori, M., & Shiogama, H. (2015). Rapid adjustments of cloud and hydrological cycle to increasing CO2: A review. *Current climate change reports*, *1*, 103–113.

Koshiro, T., Kawai, H., & Noda, A. T. (2022). Estimated cloud-top entrainment index explains positive low-cloud-cover feedback. *Proceedings of the National Academy of Sciences*, *119*(29), e2200635119.

Kuhlbrodt, T., Jones, C. G., Sellar, A., Storkey, D., Blockley, E., Stringer, M., ... others (2018). The low-resolution version of hadgem3 gc3. 1: Development and evaluation for global climate. *Journal of advances in modeling earth systems*, *10*(11), 2865–2888.

Masson-Delmotte, V., Zhai, P., Pirani, A., Connors, S. L., Péan, C., Berger, S., ... (eds.), Z. B. (2021). IPCC, 2021: Climate change 2021: The physical science basis. contribution of working group i to the sixth assessment report of the intergovernmental panel on climate change.

McKinney, W., et al. (2011). pandas: a foundational Python library for data analysis and statistics. *Python for high performance and scientific computing*, *14*(9), 1–9.

Mitchell, J. F., Wilson, C., & Cunnington, W. (1987). On CO_2 climate sensitivity and model dependence of results. *Quarterly Journal of the Royal Meteorological Society*, *113*(475), 293–322.

Myers, T. A., Scott, R. C., Zelinka, M. D., Klein, S. A., Norris, J. R., & Caldwell, P. M. (2021). Observational constraints on low cloud feedback reduce uncertainty of climate sensitivity. *Nature Climate Change*, *11*(6), 501–507.

Ogura, T., Watanabe, M., & Hirota, N. (2019). [Dataset] MIROC MIROC6 model output prepared for CMIP6 CFMIP amip-p4K. Earth System Grid Federation.
doi: https://doi.org/10.22033/ESGF/CMIP6.5446

Ogura, T., Webb, M. J., & Lock, A. P. (submitted). Positive low cloud feedback primarily caused by increasing longwave radiation from the sea surface in two versions of a climate model. *Submitted to Geophysical Review Letters, preprint available via the Earth System Science Open Archive*. doi: 10.22541/essoar.167979595.57126822/v1

Oliphant, T. E., et al. (2006). *A guide to NumPy* (Vol. 1). Trelgol Publishing USA.

Richter, I., & Xie, S.-P. (2008). Muted precipitation increase in global warming simulations: A surface evaporation perspective. *Journal of Geophysical Research: Atmospheres*, *113*(D24).

Rieck, M., Nuijens, L., & Stevens, B. (2012). Marine boundary layer cloud feedbacks in a constant relative humidity atmosphere. *Journal of the Atmospheric Sciences*, *69*(8), 2538–2550.

Rose, B. E. (2018). CLIMLAB: a Python toolkit for interactive, process-oriented climate modeling. *J. Open Source Softw.*, *3*(24), 659.

Schiro, K. A., Su, H., Ahmed, F., Dai, N., Singer, C. E., Gentine, P., ... David Neelin, J. (2022). Model spread in tropical low cloud feedback tied to overturning circulation response to warming. *Nature Communications*, *13*(1), 7119.

Sherwood, S., Webb, M. J., Annan, J. D., Armour, K. C., Forster, P. M., Hargreaves, J. C., ... others (2020). An assessment of earth's climate sensitivity using multiple lines of evidence. *Reviews of Geophysics*, *58*(4), e2019RG000678.

Sherwood, S. C., Bony, S., & Dufresne, J.-L. (2014). Spread in model climate sensitivity traced to atmospheric convective mixing. *Nature*, *505*(7481), 37–42.

Soden, B. J., Broccoli, A. J., & Hemler, R. S. (2004). On the use of cloud forcing to estimate cloud feedback. *Journal of climate*, *17*(19), 3661–3665.

Tatebe, H., Ogura, T., Nitta, T., Komuro, Y., Ogochi, K., Takemura, T., ... others (2019). Description and basic evaluation of simulated mean state, internal variability, and climate sensitivity in miroc6. *Geoscientific Model Development*, *12*(7), 2727–2765.

Teixeira, J., Cardoso, S., Bonazzola, M., Cole, J., DelGenio, A., DeMott, C., ... others (2011). Tropical and subtropical cloud transitions in weather and climate prediction models: The gcss/wgne pacific cross-section intercomparison (gpci). *Journal of Climate*, *24*(20), 5223–5256.

Vial, J., Albright, A. L., Vogel, R., Musat, I., & Bony, S. (2023). Cloud transition across the daily cycle illuminates model responses of trade cumuli to warming. *Proceedings of the National Academy of Sciences*, *120*(8), e2209805120.

Vial, J., Bony, S., Dufresne, J.-L., & Roehrig, R. (2016). Coupling between lower-tropospheric convective mixing and low-level clouds: Physical mechanisms and dependence on convection scheme. *Journal of Advances in Modeling Earth Systems*. Retrieved from `http://dx.doi.org/10.1002/2016MS000740` doi: 10.1002/2016MS000740

Webb, M. (2019). [Dataset] HadGEM3-GC31-LL model output prepared for CMIP6 CFMIP amip-p4K. Earth System Grid Federation.
doi: https://doi.org/10.22033/ESGF/CMIP6.5873

Webb, M. J. (2023). [Dataset] Software and data for "What physical mechanisms cause positive subtropical low cloud feedbacks in climate models?" submitted to JAMES.
doi: https://doi.org/10.5281/zenodo.7786930

Webb, M. J., Andrews, T., Bodas-Salcedo, A., Bony, S., Bretherton, C. S., Chadwick, R., ... others (2017). The cloud feedback model intercomparison project (cfmip) contribution to cmip6. *Geoscientific Model Development*, *2017*, 359–

384.

Webb, M. J., & Lock, A. P. (2013). Coupling between subtropical cloud feedback and the local hydrological cycle in a climate model. *Climate dynamics*, *41*(7-8), 1923–1939.

Webb, M. J., Lock, A. P., Bretherton, C. S., Bony, S., Cole, J. N., Idelkadi, A., ... others (2015). The impact of parametrized convection on cloud feedback. *Philosophical Transactions of the Royal Society A: Mathematical, Physical and Engineering Sciences*, *373*(2054), 20140414.

Wu, T., Chu, M., Dong, M., Fang, Y., Jie, W., Li, J., ... Zhang, Y. (2019). [Dataset] BCC-CSM2MR model output prepared for CMIP6 CFMIP amip-p4k. Earth System Grid Federation. doi: https://doi.org/10.22033/ESGF/CMIP6.2864

Wu, T., Lu, Y., Fang, Y., Xin, X., Li, L., Li, W., ... others (2019). The beijing climate center climate system model (bcc-csm): the main progress from cmip5 to cmip6. *Geoscientific Model Development*, *12*(4), 1573–1600.

Wyant, M. C., Bretherton, C. S., Rand, H. A., & Stevens, D. E. (1997). Numerical simulations and a conceptual model of the stratocumulus to trade cumulus transition. *Journal of the atmospheric sciences*, *54*(1), 168–192.

Yukimoto, S., Kawai, H., Koshiro, T., Oshima, N., Yoshida, K., Urakawa, S., ... others (2019). The meteorological research institute earth system model version 2.0, mri-esm2. 0: Description and basic evaluation of the physical component. *Journal of the Meteorological Society of Japan. Ser. II*.

Yukimoto, S., Koshiro, T., Kawai, H., Oshima, N., Yoshida, K., Urakawa, S., ... Adachi, Y. (2019). [Dataset] MRI MRI-ESM2.0 model output prepared for CMIP6 CFMIP amip-p4K. Earth System Grid Federation. doi: doi:https://doi.org/10.22033/ESGF/CMIP6.6771

Zhang, M., Bretherton, C. S., Blossey, P. N., Austin, P. H., Bacmeister, J. T., Bony, S., ... others (2013). CGILS: Results from the first phase of an international project to understand the physical mechanisms of low cloud feedbacks in single column models. *Journal of Advances in Modeling Earth Systems*, *5*(4), 826–842.

Figure 1.

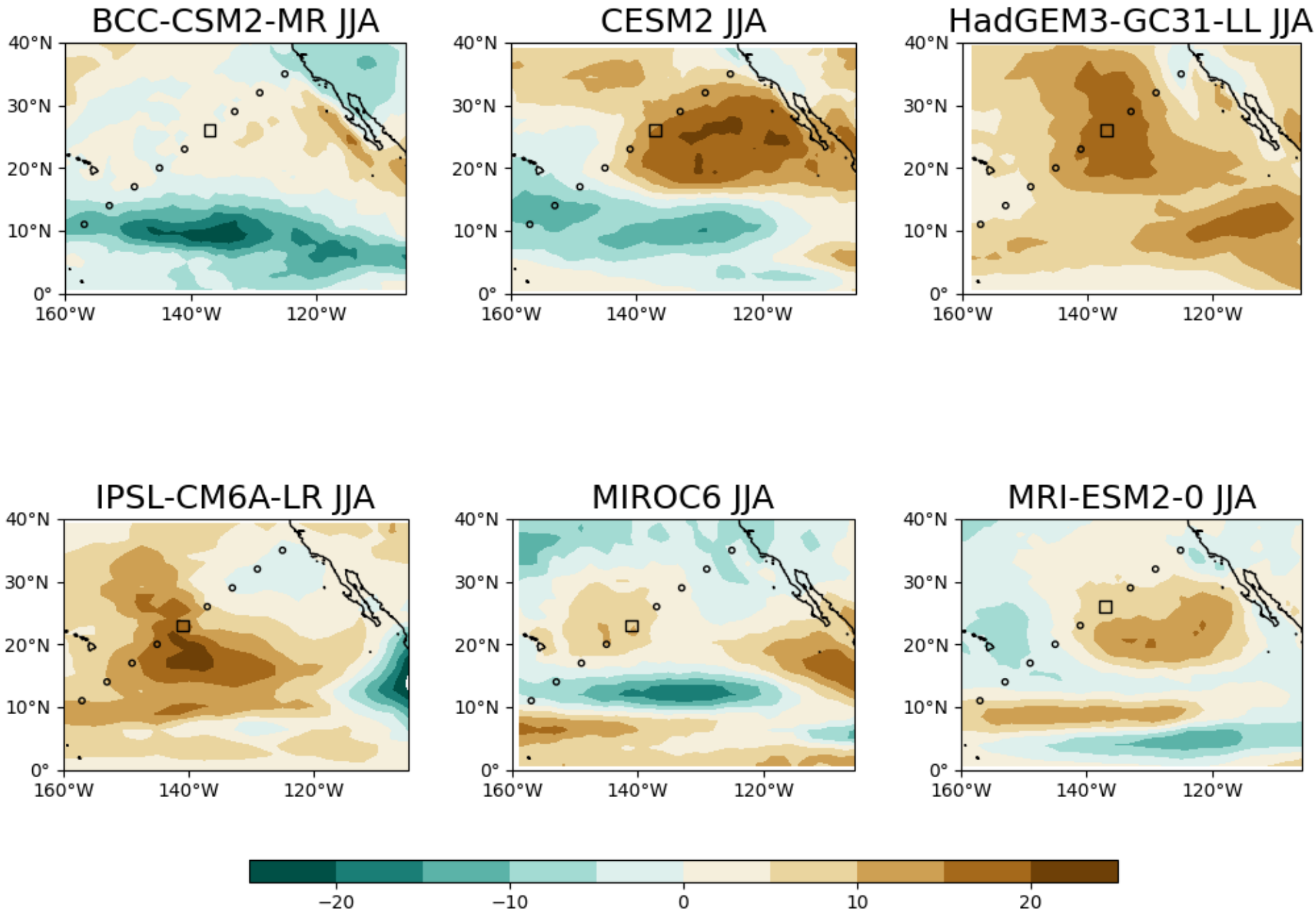
BCC-CSM2-MR JJA
CESM2 JJA
HadGEM3-GC31-LL JJA
IPSL-CM6A-LR JJA
MIROC6 JJA
MRI-ESM2-0 JJA
40°N
30°N
20°N
10°N
0°
160°W
140°W
120°W
−20
−10
0
10
20

Figure 2.

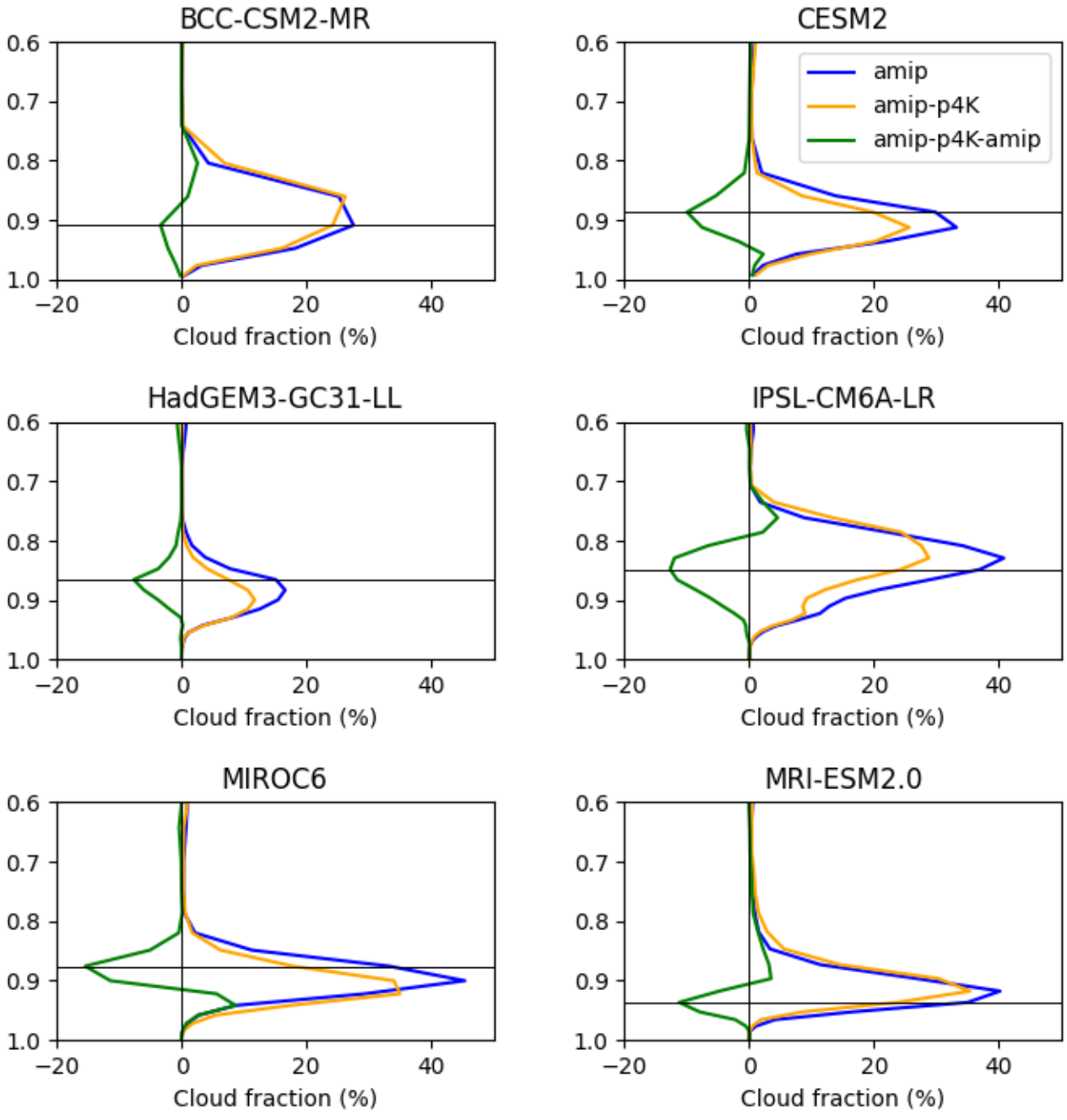
BCC-CSM2-MR
CESM2
HadGEM3-GC31-LL
IPSL-CM6A-LR
MIROC6
MRI-ESM2.0
amip
amip-p4K
amip-p4K-amip
0.6
0.7
0.8
0.9
1.0
−20
0
20
40
Cloud fraction (%)

Figure 3.

⇑ Sea Surface Temperature

+

⇑ Surface Latent Heat Flux

+

⇑ Cloud Layer Buoyancy and Latent Heat Flux

+ +

⇑ Turbulent Cloud Top Entrainment

⇑ Convective Detrainment into Stratocumulus

+ +

⇑ PBL depth

⇑ Negative Bouyancy Fluxes Below Cloud Base

+

⇑ Subcloud Layer Stability

+

⇑ PBL Decoupling

-

⇓ Cloud Layer Turbulent Moistening

+

⇓ Cloud Layer Relative Humidity

+

⇓ Cloud Fraction

- -

Figure 4.

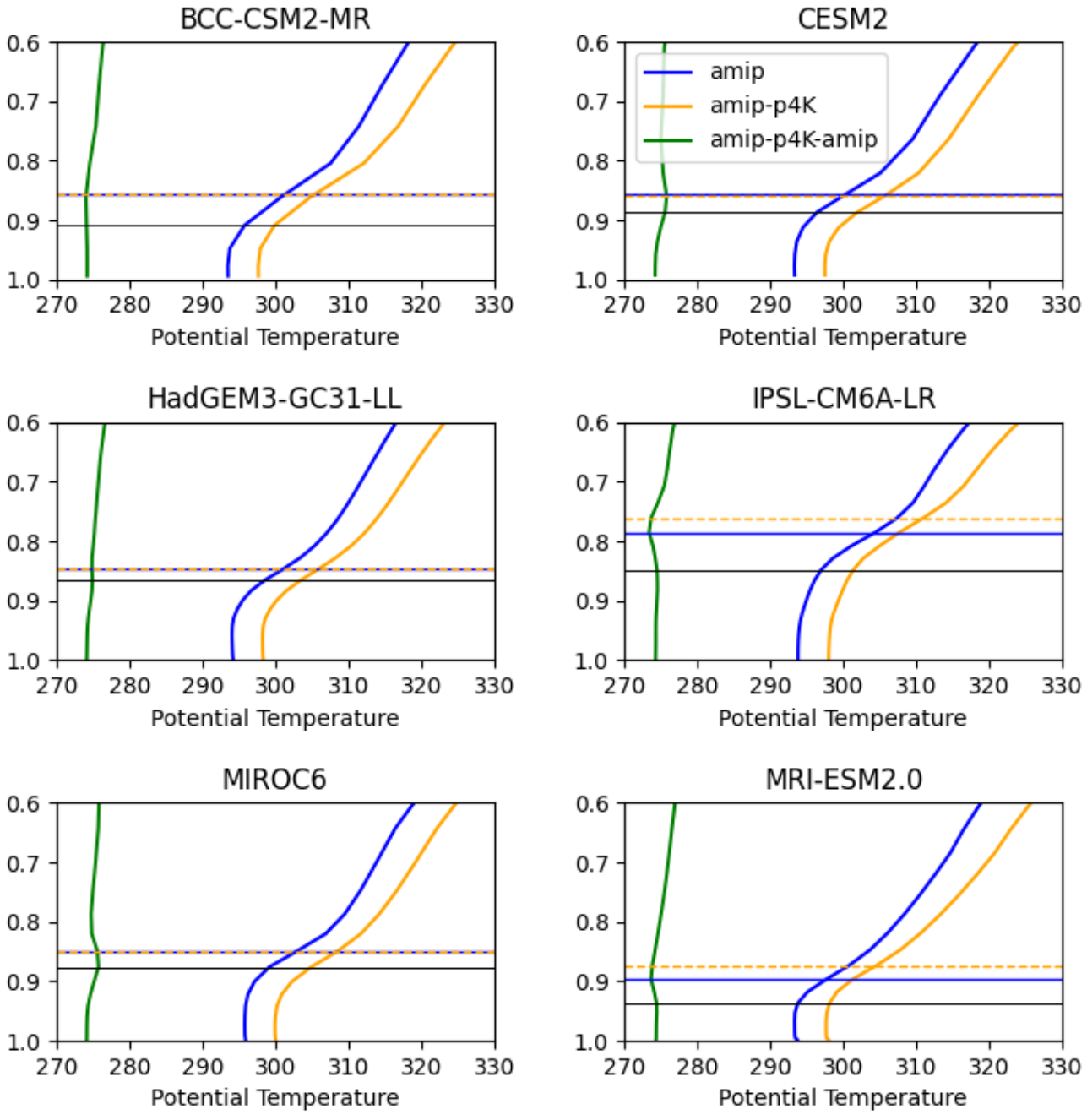
BCC-CSM2-MR
CESM2
HadGEM3-GC31-LL
IPSL-CM6A-LR
MIROC6
MRI-ESM2.0
amip
amip-p4K
amip-p4K-amip
0.6
0.7
0.8
0.9
1.0
270
280
290
300
310
320
330
Potential Temperature

Figure 5.

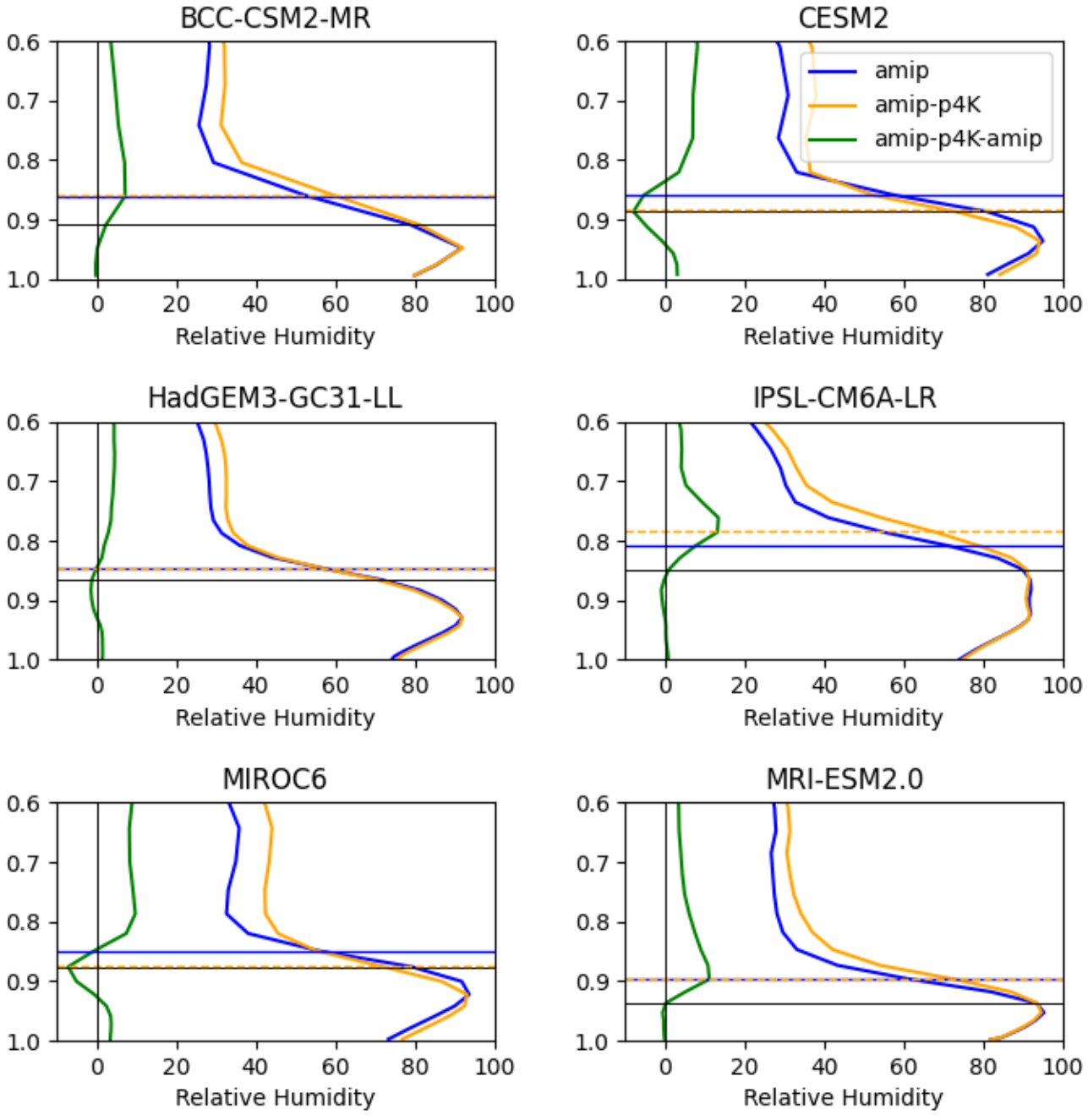
BCC-CSM2-MR
CESM2
HadGEM3-GC31-LL
IPSL-CM6A-LR
MIROC6
MRI-ESM2.0
amip
amip-p4K
amip-p4K-amip
0.6
0.7
0.8
0.9
1.0
0
20
40
60
80
100
Relative Humidity

Figure 6.

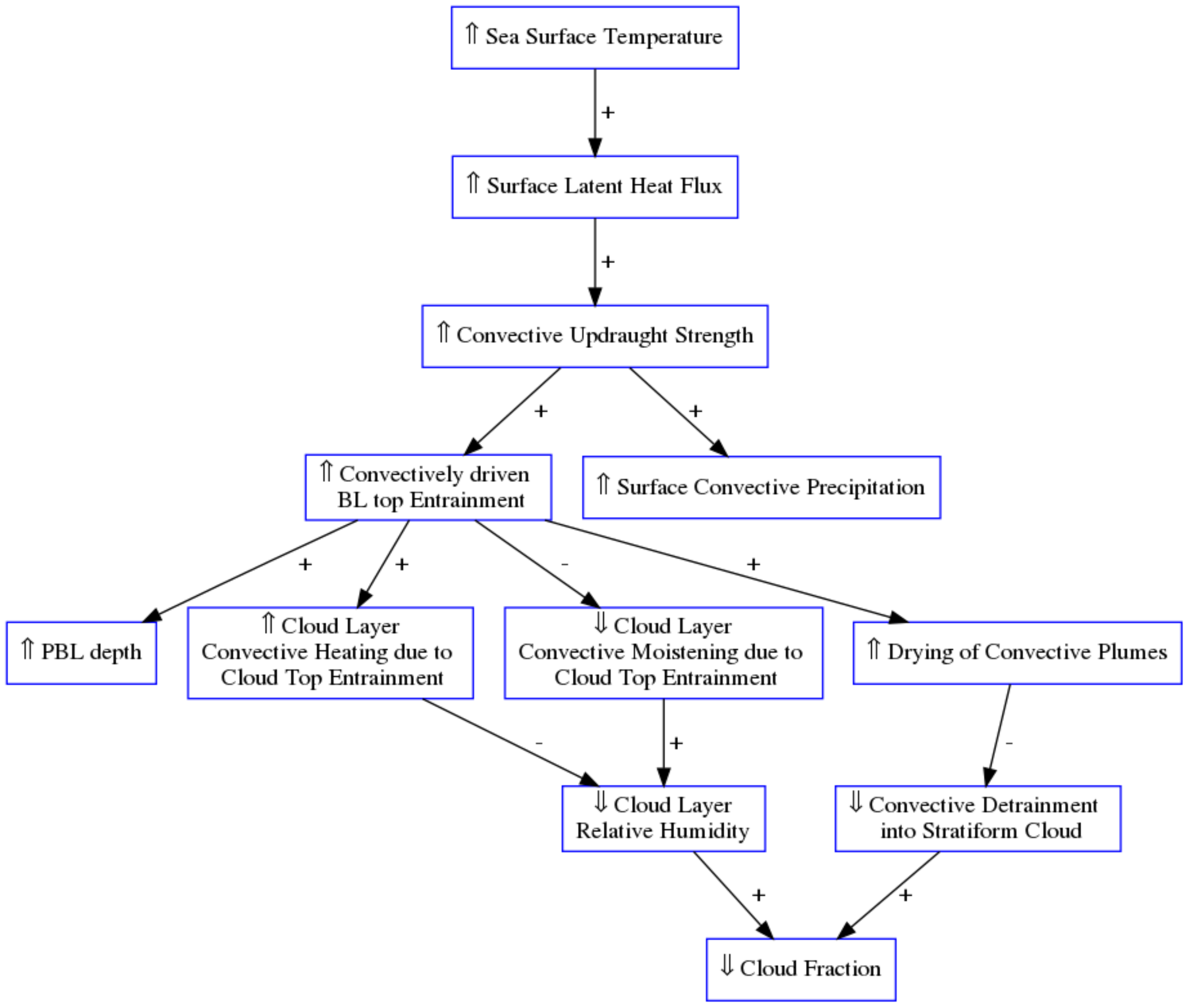
⇑ Sea Surface Temperature
+
⇑ Surface Latent Heat Flux
+
⇑ Convective Updraught Strength
+
+
⇑ Convectively driven
BL top Entrainment
⇑ Surface Convective Precipitation
+
+
-
+
⇑ PBL depth
⇑ Cloud Layer
Convective Heating due to
Cloud Top Entrainment
⇓ Cloud Layer
Convective Moistening due to
Cloud Top Entrainment
⇑ Drying of Convective Plumes
-
+
-
⇓ Cloud Layer
Relative Humidity
⇓ Convective Detrainment
into Stratiform Cloud
+
+
⇓ Cloud Fraction

Figure 7.

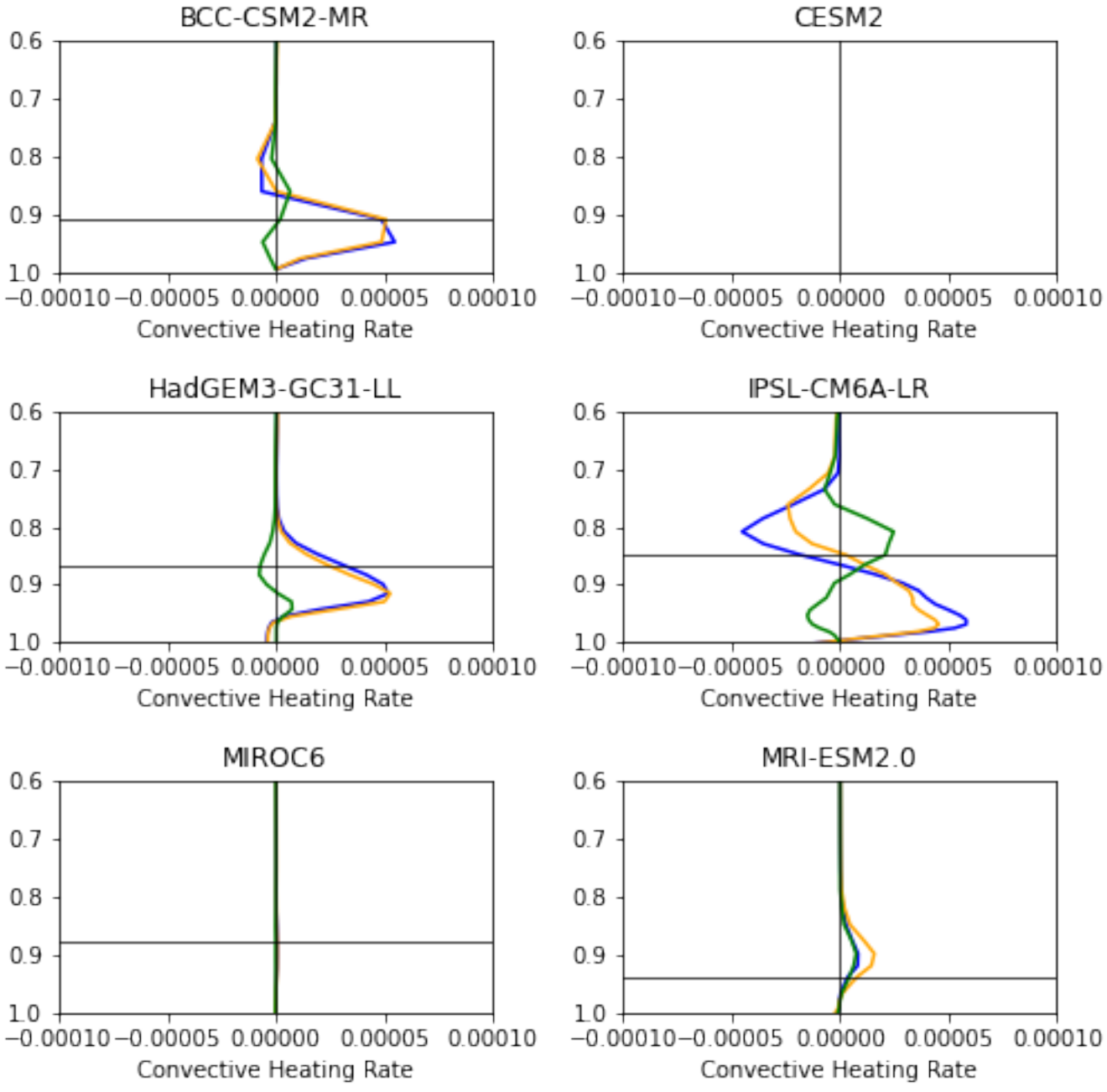
BCC-CSM2-MR
CESM2
HadGEM3-GC31-LL
IPSL-CM6A-LR
MIROC6
MRI-ESM2.0
0.6
0.7
0.8
0.9
1.0
−0.00010
−0.00005
0.00000
0.00005
0.00010
Convective Heating Rate

Figure 8.

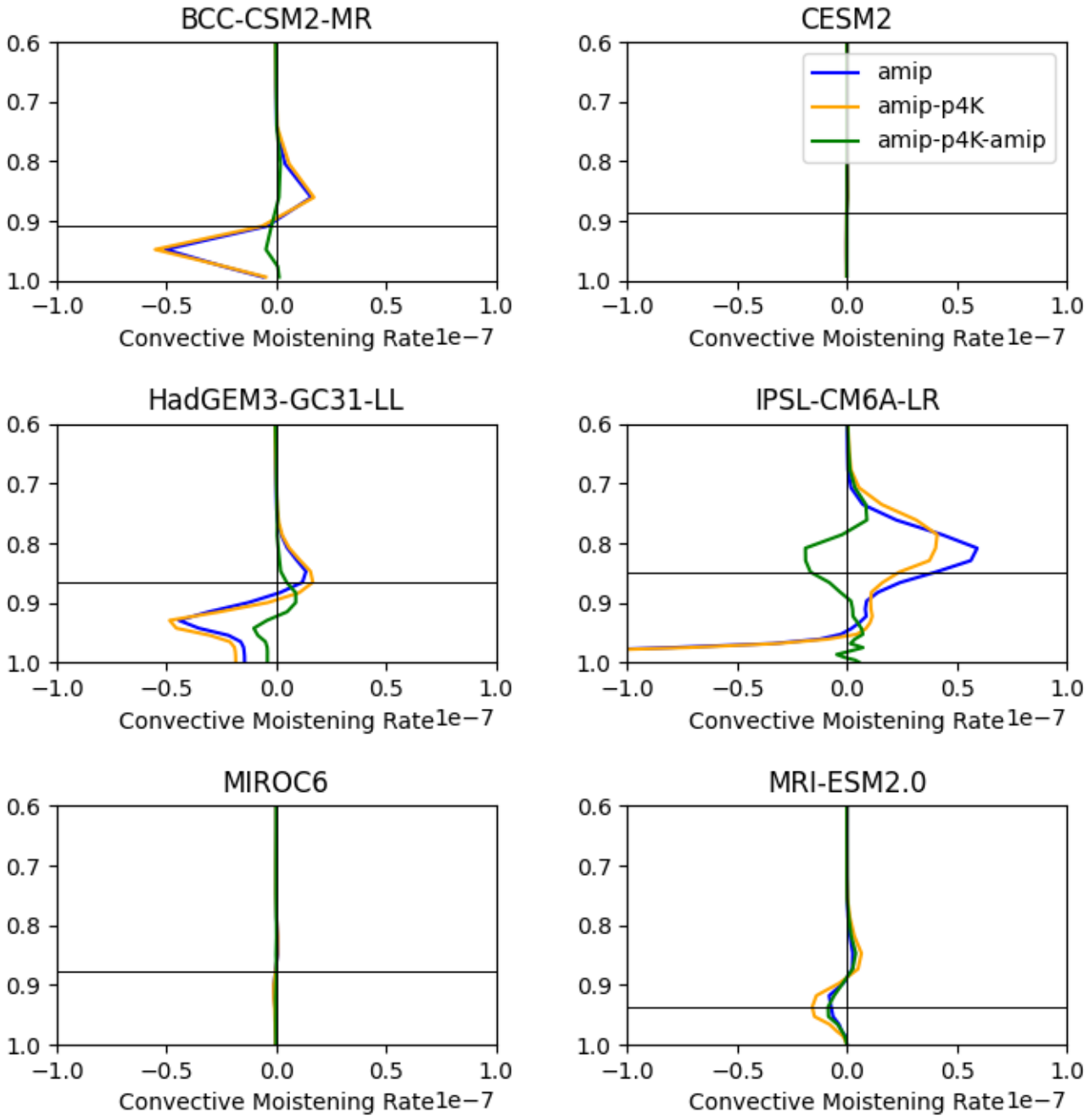
BCC-CSM2-MR
CESM2
HadGEM3-GC31-LL
IPSL-CM6A-LR
MIROC6
MRI-ESM2.0
amip
amip-p4K
amip-p4K-amip
0.6
0.7
0.8
0.9
1.0
−1.0
−0.5
0.0
0.5
1.0
Convective Moistening Rate
1e−7

Figure 9.

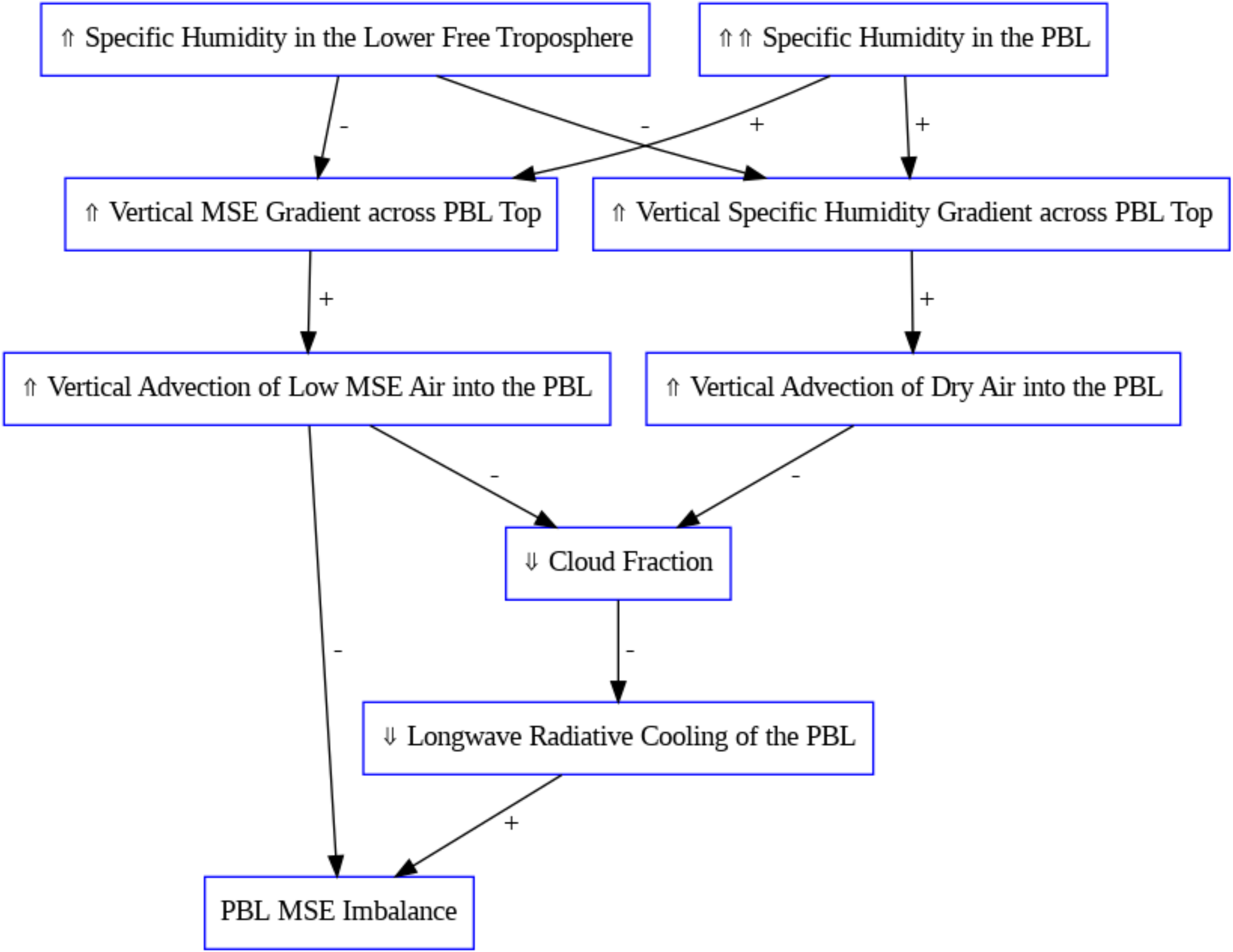
⇑ Specific Humidity in the Lower Free Troposphere
⇑⇑ Specific Humidity in the PBL
-
-
+
+
⇑ Vertical MSE Gradient across PBL Top
⇑ Vertical Specific Humidity Gradient across PBL Top
+
+
⇑ Vertical Advection of Low MSE Air into the PBL
⇑ Vertical Advection of Dry Air into the PBL
-
-
⇓ Cloud Fraction
-
-
⇓ Longwave Radiative Cooling of the PBL
+
PBL MSE Imbalance

Figure 10.

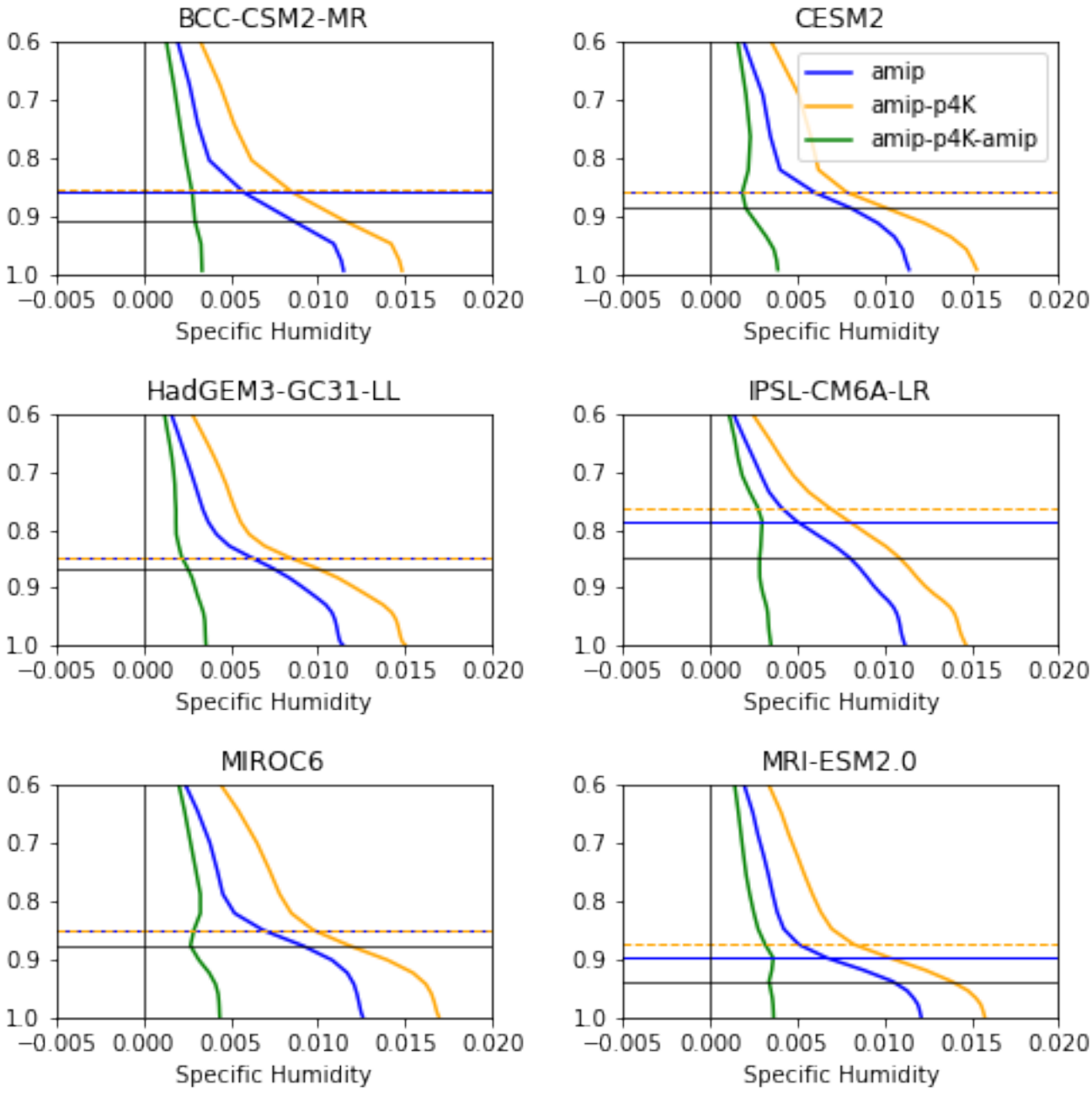
BCC-CSM2-MR
CESM2
HadGEM3-GC31-LL
IPSL-CM6A-LR
MIROC6
MRI-ESM2.0
amip
amip-p4K
amip-p4K-amip
0.6
0.7
0.8
0.9
1.0
−0.005
0.000
0.005
0.010
0.015
0.020
Specific Humidity

Figure 11.

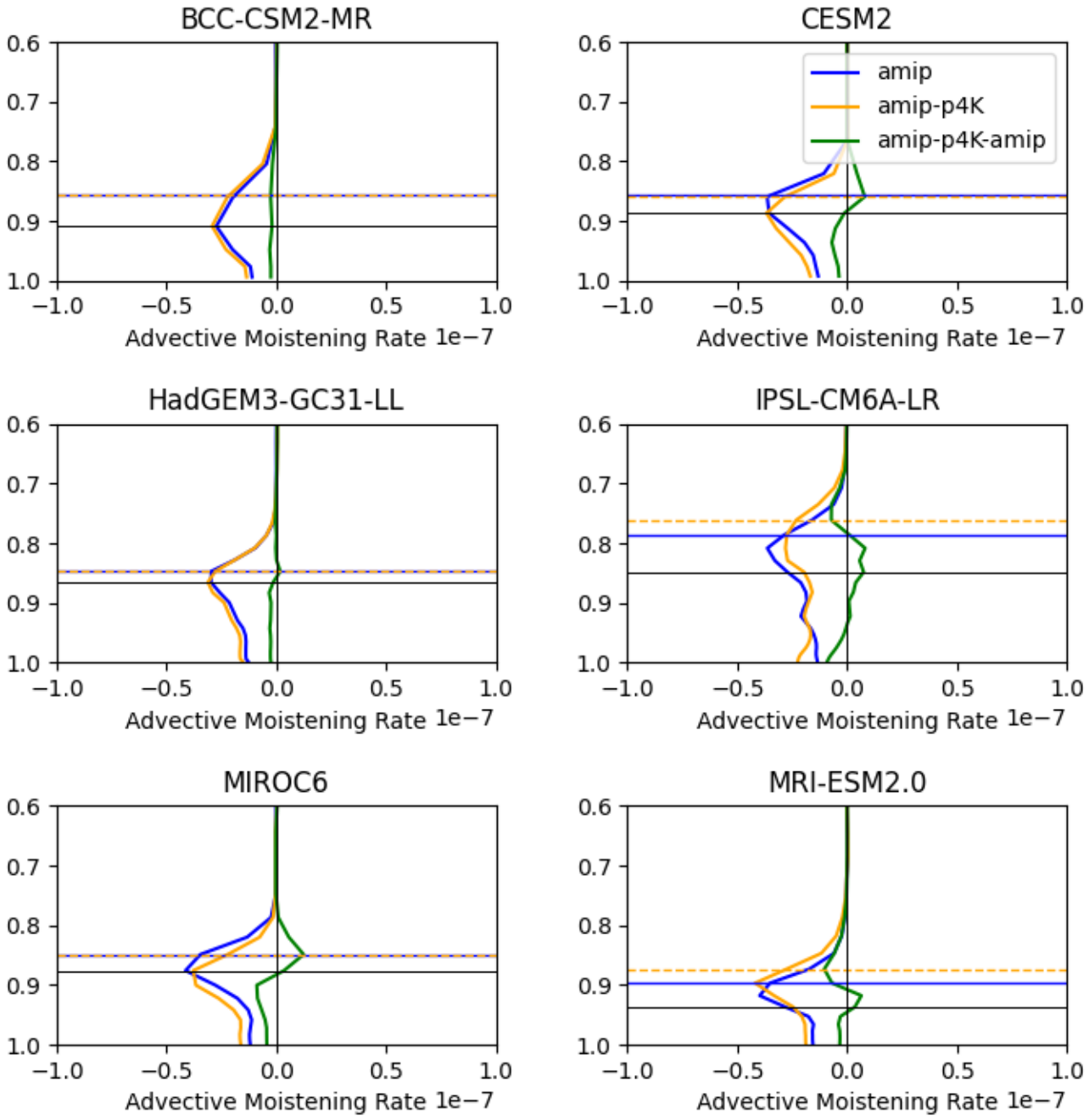
BCC-CSM2-MR
CESM2
HadGEM3-GC31-LL
IPSL-CM6A-LR
MIROC6
MRI-ESM2.0
amip
amip-p4K
amip-p4K-amip
0.6
0.7
0.8
0.9
1.0
−1.0
−0.5
0.0
0.5
1.0
Advective Moistening Rate 1e−7

Figure 12.

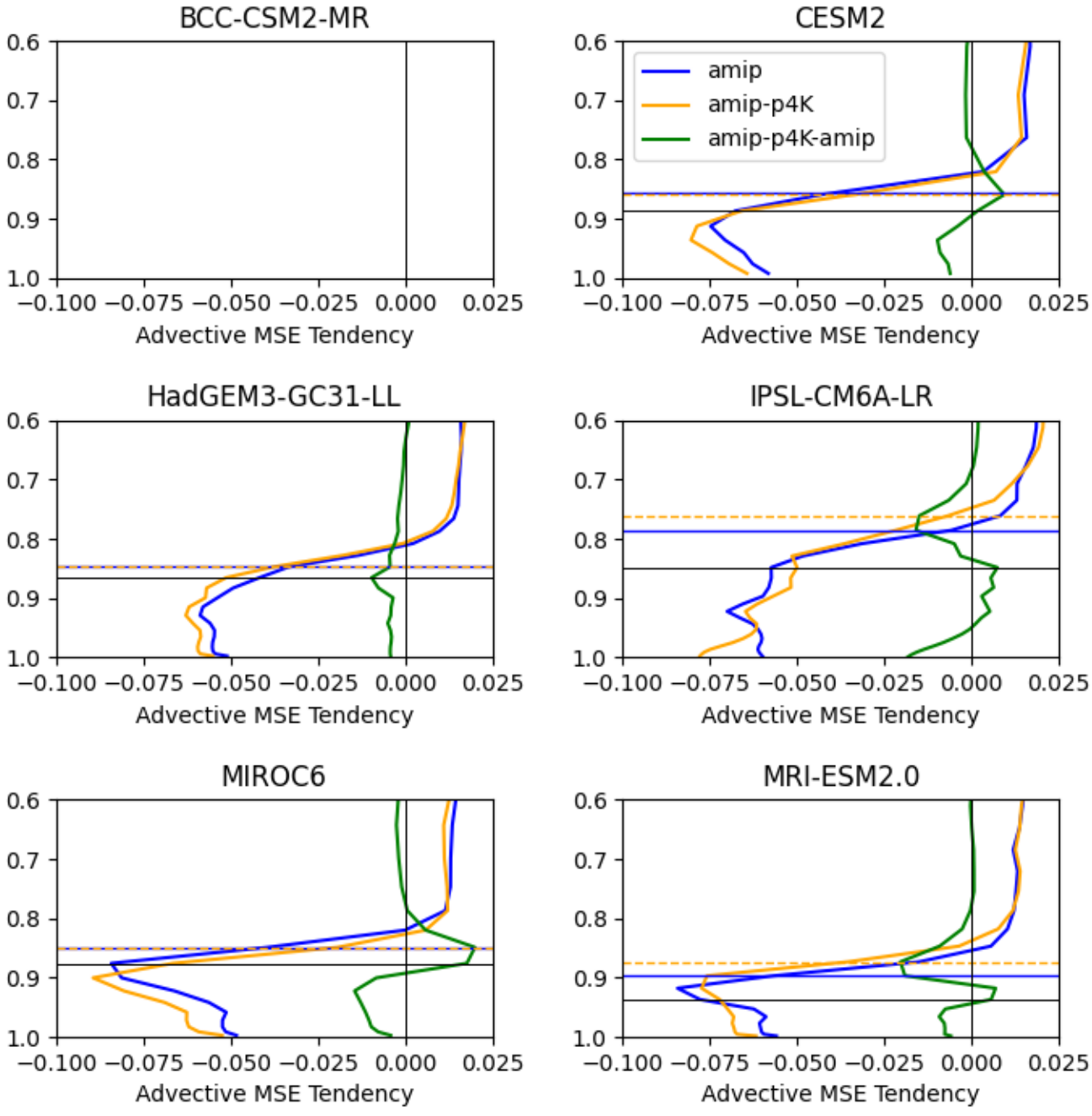
BCC-CSM2-MR
CESM2
HadGEM3-GC31-LL
IPSL-CM6A-LR
MIROC6
MRI-ESM2.0
amip
amip-p4K
amip-p4K-amip
0.6
0.7
0.8
0.9
1.0
−0.100 −0.075 −0.050 −0.025 0.000 0.025
Advective MSE Tendency

Figure 13.

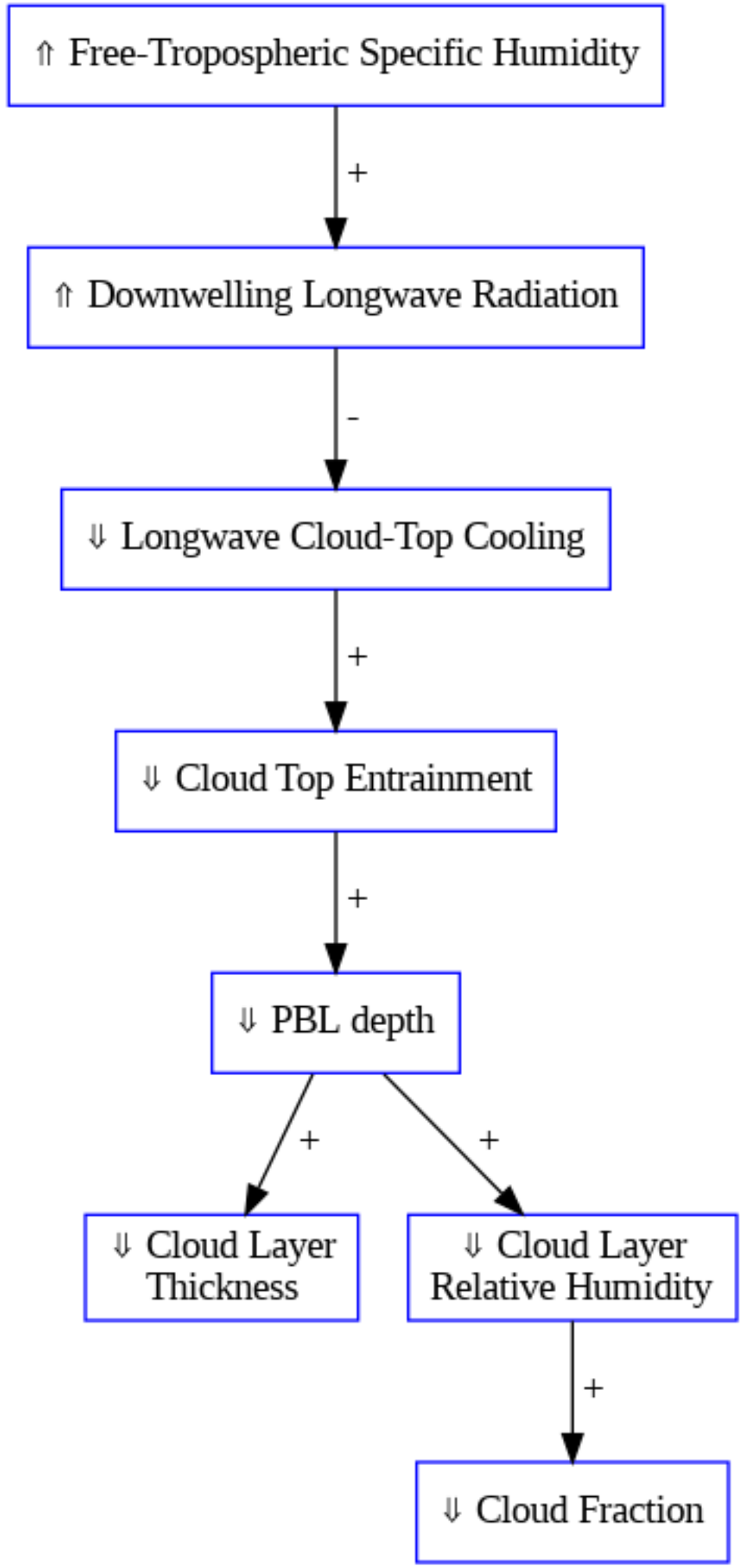
⇑ Free-Tropospheric Specific Humidity
+
⇑ Downwelling Longwave Radiation
-
⇓ Longwave Cloud-Top Cooling
+
⇓ Cloud Top Entrainment
+
⇓ PBL depth
+
+
⇓ Cloud Layer Thickness
⇓ Cloud Layer Relative Humidity
+
⇓ Cloud Fraction

Figure 14.

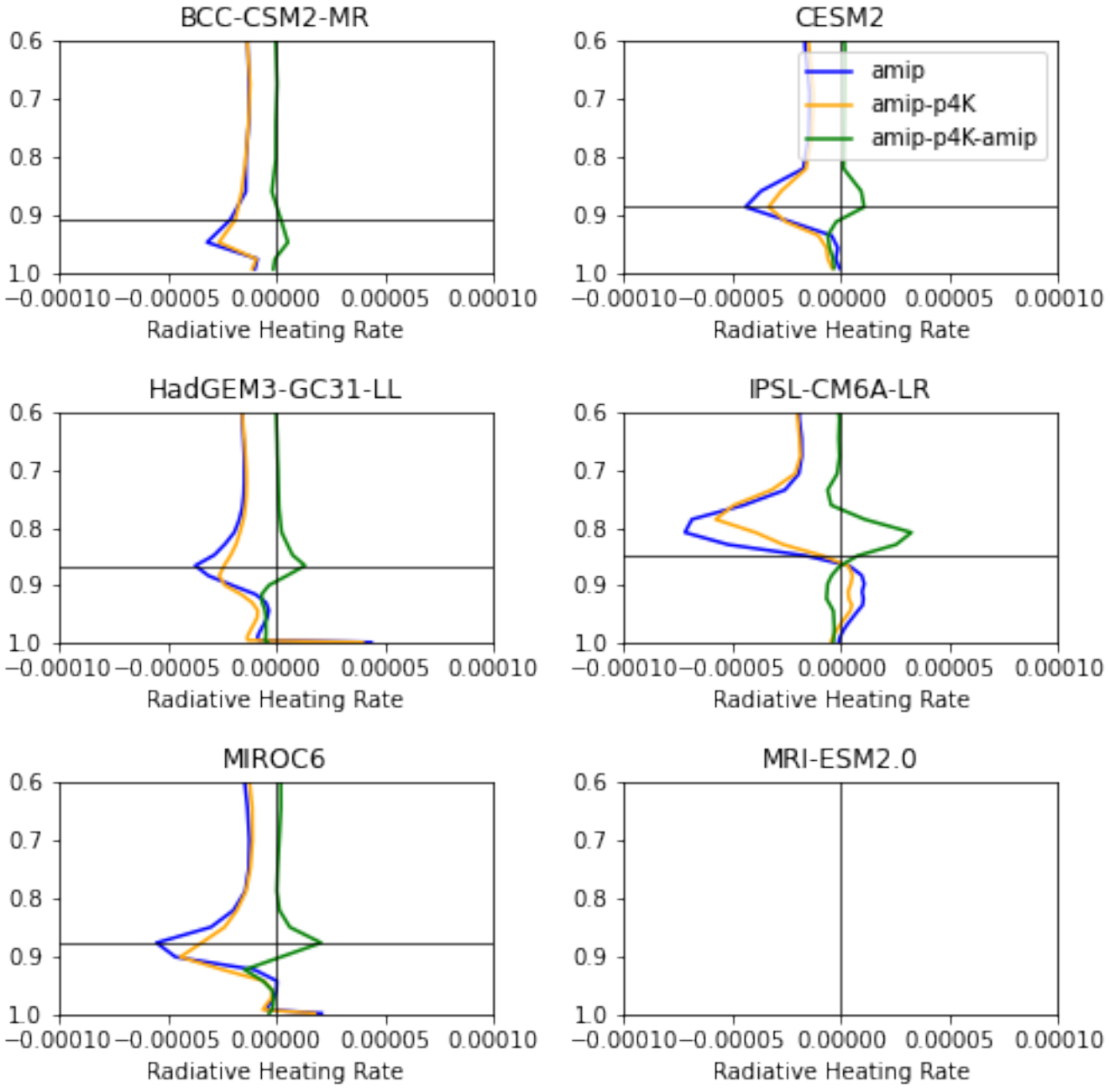
BCC-CSM2-MR
CESM2
HadGEM3-GC31-LL
IPSL-CM6A-LR
MIROC6
MRI-ESM2.0
amip
amip-p4K
amip-p4K-amip
0.6
0.7
0.8
0.9
1.0
−0.00010
−0.00005
0.00000
0.00005
0.00010
Radiative Heating Rate

Figure 15.

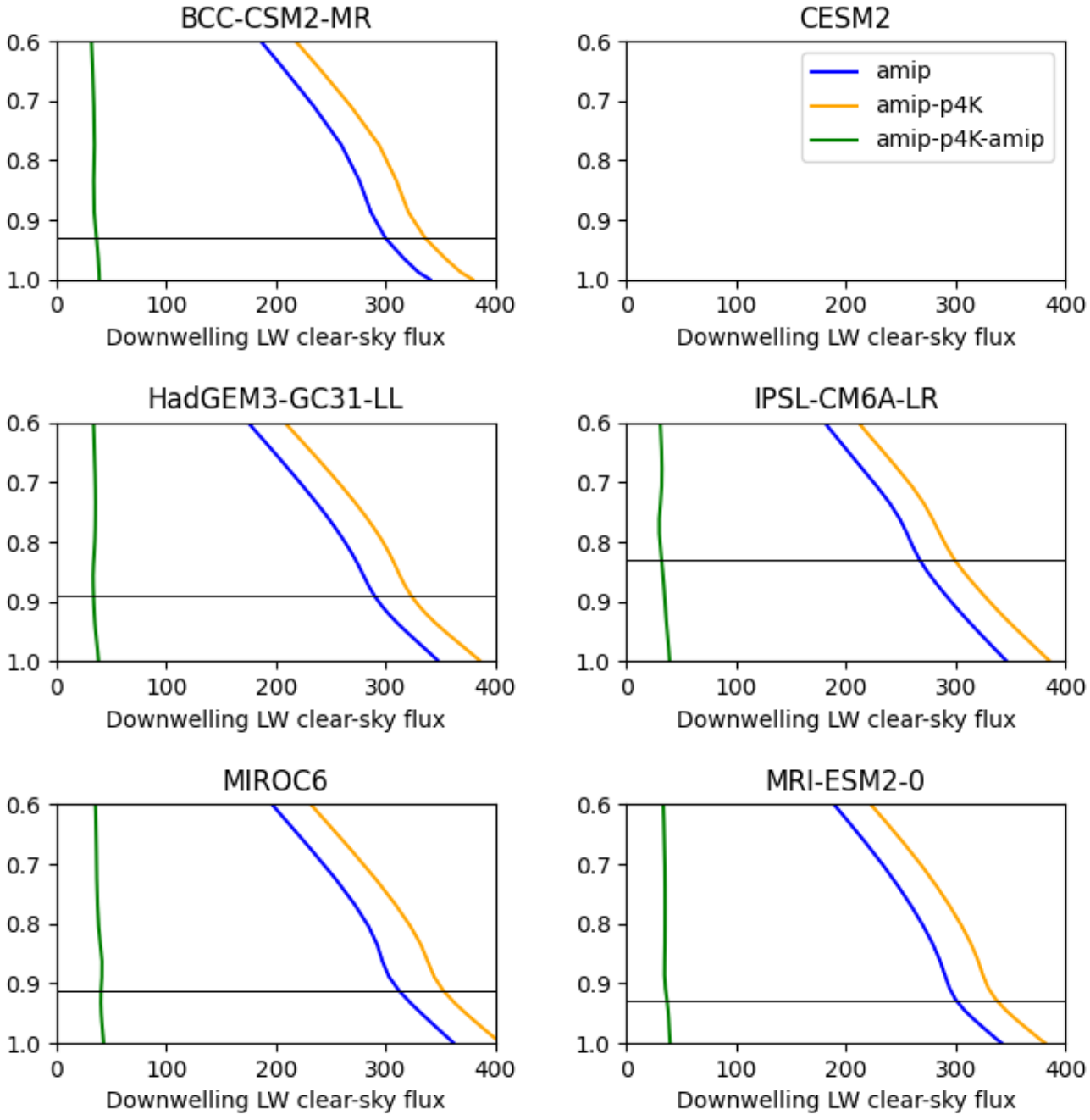
BCC-CSM2-MR
CESM2
HadGEM3-GC31-LL
IPSL-CM6A-LR
MIROC6
MRI-ESM2-0
amip
amip-p4K
amip-p4K-amip
0.6
0.7
0.8
0.9
1.0
0
100
200
300
400
Downwelling LW clear-sky flux

Figure 16.

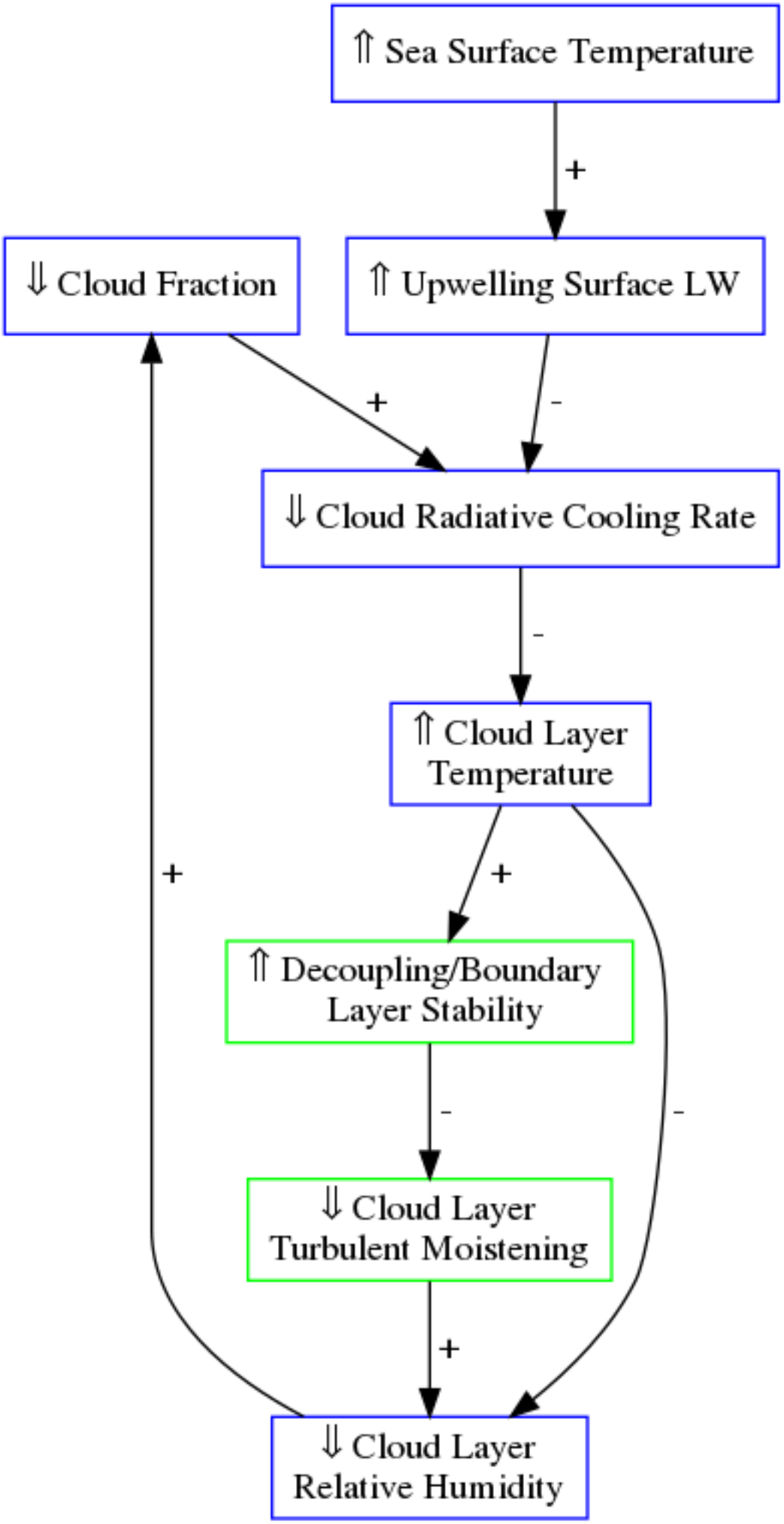
⇑ Sea Surface Temperature
+
⇓ Cloud Fraction
⇑ Upwelling Surface LW
+
-
⇓ Cloud Radiative Cooling Rate
-
⇑ Cloud Layer Temperature
+
+
⇑ Decoupling/Boundary Layer Stability
-
-
⇓ Cloud Layer Turbulent Moistening
+
⇓ Cloud Layer Relative Humidity

Figure 17.

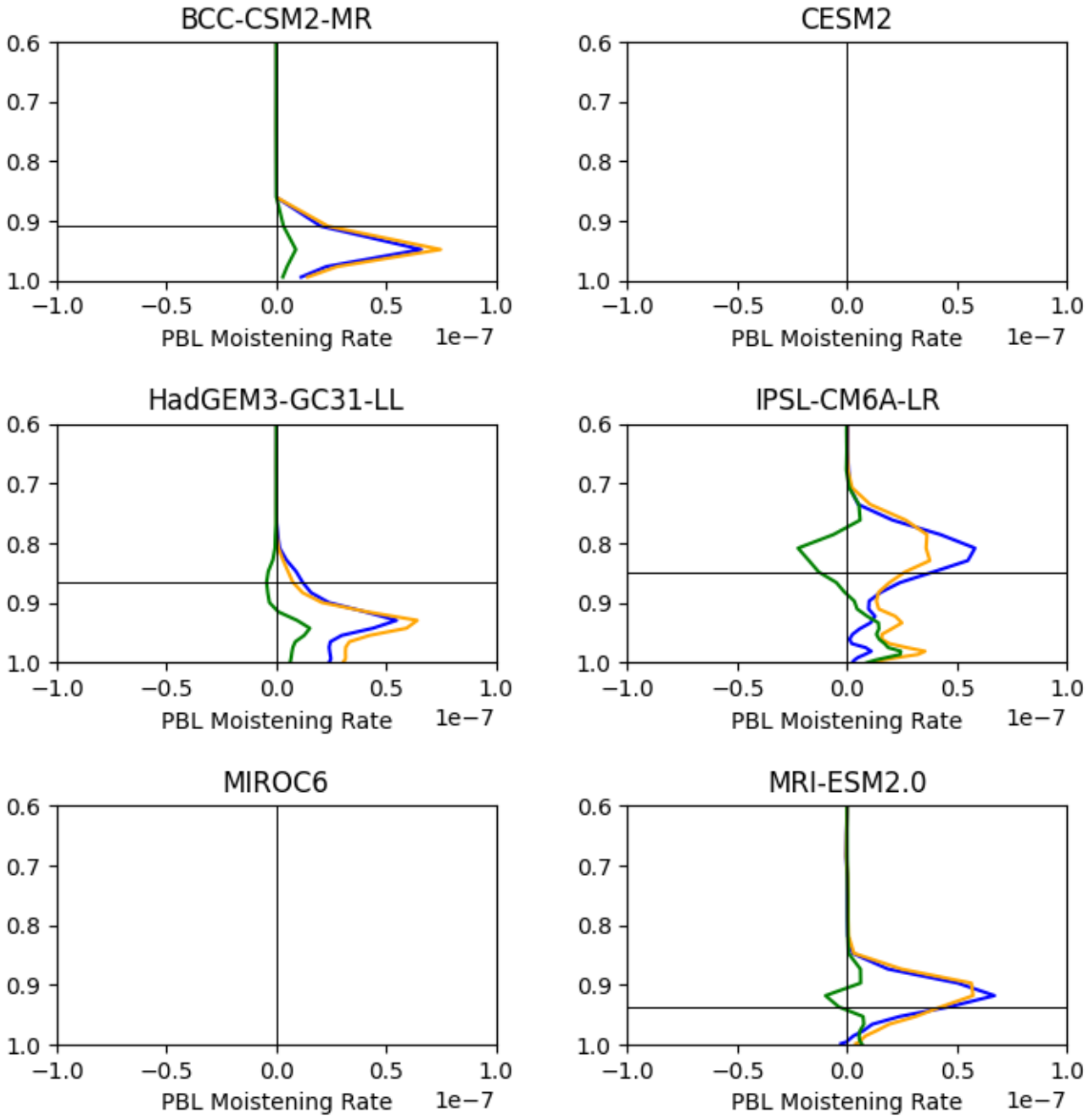
BCC-CSM2-MR
CESM2
HadGEM3-GC31-LL
IPSL-CM6A-LR
MIROC6
MRI-ESM2.0
0.6
0.7
0.8
0.9
1.0
−1.0
−0.5
0.0
0.5
1.0
PBL Moistening Rate
1e−7

Figure 18.

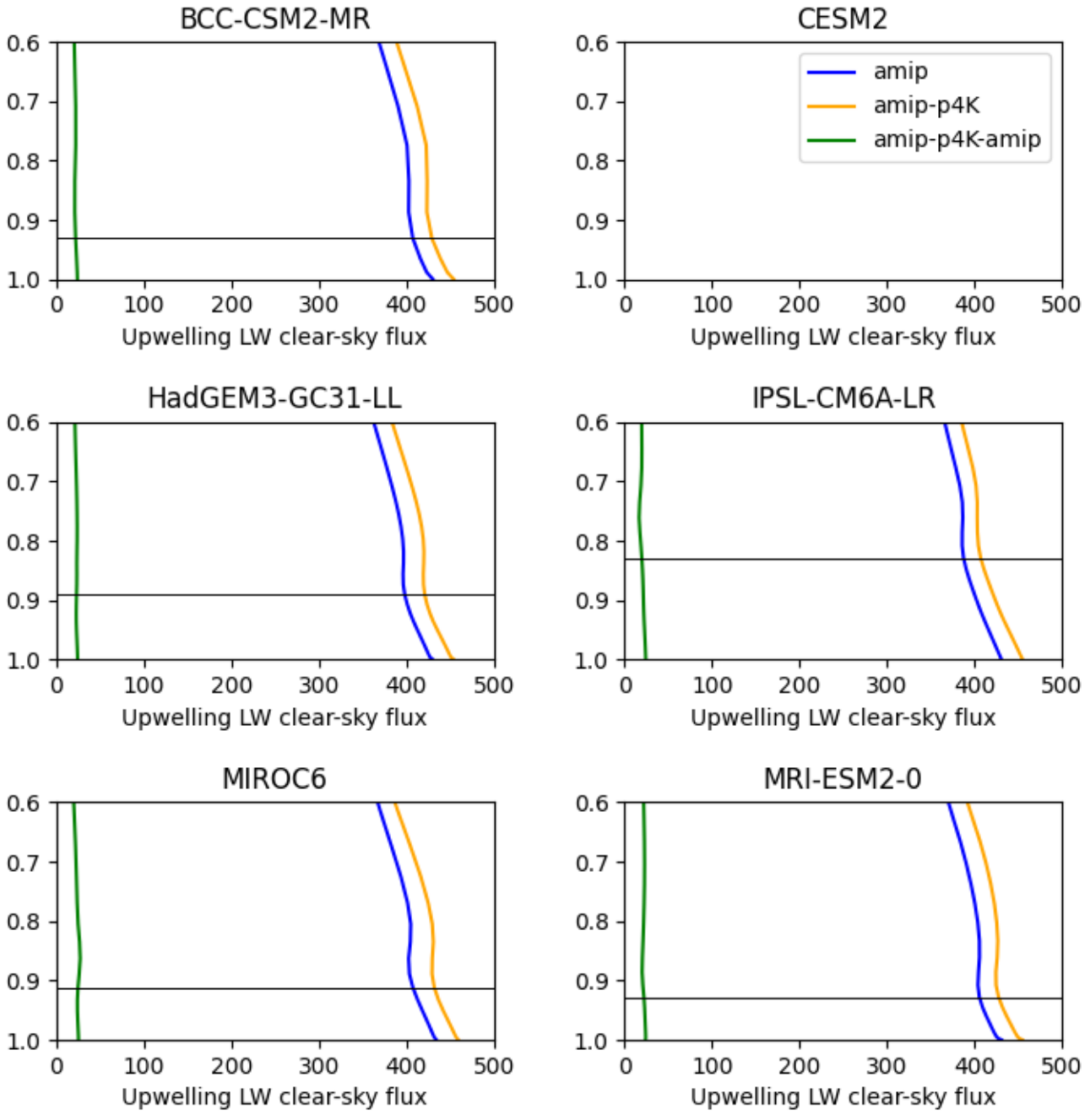
BCC-CSM2-MR
CESM2
HadGEM3-GC31-LL
IPSL-CM6A-LR
MIROC6
MRI-ESM2-0
amip
amip-p4K
amip-p4K-amip
0.6
0.7
0.8
0.9
1.0
0
100
200
300
400
500
Upwelling LW clear-sky flux